Journal Pre-proof

BET Inhibition Blocks Inflammation-Induced Cardiac Dysfunction and SARS-CoV-2 Infection

Richard J. Mills, Sean J. Humphrey, Patrick RJ. Fortuna, Mary Lor, Simon R. Foster, Gregory A. Quaife-Ryan, Rebecca L. Johnston, Troy Dumenil, Cameron Bishop, Rajeev Ruraraju, Daniel J. Rawle, Thuy Le, Wei Zhao, Leo Lee, Charley Mackenzie-Kludas, Neda R. Mehdiabadi, Christopher Halliday, Dean Gilham, Li Fu, Stephen J. Nicholls, Jan Johansson, Michael Sweeney, Norman C.W. Wong, Ewelina Kulikowski, Kamil A. Sokolowski, Brian W.C. Tse, Lynn Devilée, Holly K. Voges, Liam T. Reynolds, Sophie Krumeich, Ellen Mathieson, Dad Abu-Bonsrah, Kathy Karavendzas, Brendan Griffen, Drew Titmarsh, David A. Elliott, James McMahon, Andreas Suhrbier, Kanta Subbarao, Enzo R. Porrello, Mark J. Smyth, Christian R. Engwerda, Kelli PA. MacDonald, Tobias Bald, David E. James, James E. Hudson

1 **TITLE**

2 **BET Inhibition Blocks Inflammation-Induced Cardiac Dysfunction and SARS-CoV-2**
3 **Infection**

4 **AUTHOR LIST AND AFFILIATIONS**

5 Richard J Mills[1], Sean J Humphrey[2], Patrick RJ Fortuna[1], Mary Lor[1], Simon R Foster[1],Gregory A
6 Quaife-Ryan[1], Rebecca L. Johnston[1], Troy Dumenil[1], Cameron Bishop[1], Rajeev Ruraraju[3,4,5],
7 Daniel J Rawle[1], Thuy Le[1] Wei Zhao[5], Leo Lee[5], Charley Mackenzie-Kludas[5], Neda R
8 Mehdiabadi[6], Christopher Halliday[7], Dean Gilham[7], Li Fu[7], Stephen J. Nicholls[8], Jan
9 Johansson[9], Michael Sweeney[9], Norman C.W. Wong[7], Ewelina Kulikowski[7], Kamil A.
10 Sokolowski[10], Brian W. C. Tse[10], Lynn Devilée[1], Holly K Voges[1], Liam T Reynolds[1], Sophie
11 Krumeich[1], Ellen Mathieson[1], Dad Abu-Bonsrah[6,11], Kathy Karavendzas[6], Brendan Griffen[12],
12 Drew Titmarsh[12], David A Elliott[6], James McMahon[13,14], Andreas Suhrbier[1,15], Kanta
13 Subbarao[3,5], Enzo R Porrello[6,16], Mark J Smyth[1], Christian R Engwerda[1], Kelli PA MacDonald[1],
14 Tobias Bald[1,18], David E James[2], James E Hudson[1,*]

15 [1]QIMR Berghofer Medical Research Institute, Brisbane, 4006, QLD, Australia
16 [2] Charles Perkins Centre, School of Life and Environmental Science, The University of Sydney,
17 Sydney, 2006, NSW, Australia
18 [3]The WHO Collaborating Centre for Reference and Research on Influenza, The Peter Doherty
19 Institute for Infection and Immunity, Melbourne, 3000, VIC, Australia
20 [4]Department of Microbiology and Immunology, The University of Melbourne, Melbourne, 3052,
21 VIC, Australia
22 [5]The Peter Doherty Institute for Infection and Immunity, Melbourne, 3000, VIC, Australia
23 [6]Murdoch Children's Research Institute, The Royal Children's Hospital, Melbourne, 3052, VIC,
24 Australia
25 [7]Resverlogix Corp., Calgary, T3E 6L1. AB, Canada
26 [8]Victorian Heart Hospital, Monash University, Clayton, 3168, VIC, Australia
27 [9]Resverlogix Corp., San Francisco, 94104, CA, USA
28 [10]Preclinical Imaging Facility, Translational Research Institute, Brisbane, Australia
29 [11]Department of Paediatrics, The University of Melbourne, Melbourne, 3052, VIC, Australia
30 [12]Dynomics Inc., San Mateo, 94401, CA, USA and Dynomics Pty Ltd, Brisbane, 4000, QLD,
31 Australia
32 [13]Department of Infectious Diseases, Alfred Hospital and Monash University, Melbourne, 3004,
33 VIC, Australia
34 [14]Department of Infectious Diseases, Monash Medical Centre, Clayton, 3168, VIC, Australia
35 [15]GVN Center of Excellence, Australian Infectious Diseases Research Centre, Brisbane, QLD,
36 Australia
37 [16]Department of Physiology, School of Biomedical Sciences, The University of Melbourne,
38 Melbourne, 3052, VIC, Australia
39 [17]Faculty of Medicine and Health, The University of Sydney, Sydney, 2006, NSW, Australia
40 [18]Institute of Experimental Oncology, University Hospital Bonn, 53127, Bonn, Germany
41
42 *Lead contact and corresponding author:
43 Associate Professor James E. Hudson
44 QIMR Berghofer Medical Research Institute
45 Herston, Brisbane
46 QLD, 4006, Australia
47 Tel: +61 7 3362 0141
48 Email: james.hudson@qimrberghofer.edu.au

1   **SUMMARY**

2   Cardiac injury and dysfunction occur in COVID-19 patients and increase the risk of mortality.
3   Causes are ill defined, but could be direct cardiac infection and/or inflammation-induced
4   dysfunction. To identify mechanisms and cardio-protective drugs, we use a state-of-the-art
5   pipeline combining human cardiac organoids with phosphoproteomics and single nuclei RNA
6   sequencing. We identify an inflammatory 'cytokine-storm', a cocktail of interferon gamma,
7   interleukin 1β and poly(I:C), induced diastolic dysfunction. Bromodomain-containing protein 4 is
8   activated along with a viral response that is consistent in both human cardiac organoids and
9   hearts of SARS-CoV-2 infected K18-hACE2 mice. Bromodomain and extraterminal family
10   inhibitors (BETi) recover dysfunction in hCO and completely prevent cardiac dysfunction and
11   death in a mouse cytokine-storm model. Additionally, BETi decreases transcription of genes in
12   the viral response, decreases ACE2 expression and reduces SARS-CoV-2 infection of
13   cardiomyocytes. Together, BETi, including the FDA breakthrough designated drug apabetalone,
14   are promising candidates to prevent COVID-19 mediated cardiac damage.

1 **INTRODUCTION**

2 SARS-CoV-2 infection leads to cardiac injury and dysfunction in 20-30% of hospitalized patients
3 (Guo et al., 2020) and higher rates of mortality in patients with pre-existing cardiovascular
4 disease (Shi et al., 2020; Wu and McGoogan, 2020). The cardiac sequelae reported in patients
5 with COVID-19, include acute coronary syndromes, cardiomyopathy, acute pulmonary heart
6 disease, arrhythmias and heart failure (Gupta et al., 2020). Furthermore, 68-78% have
7 sustained cardiac dysfunction, primarily right ventricle dysfunction and left ventricular diastolic
8 dysfunction (Puntmann et al., 2020; Szekely et al., 2020). Yet clear mechanistic insight is
9 currently lacking.

10 In the absence of infection, well known inflammatory mediators such as TNF are associated
11 with heart failure and have been demonstrated to induce systolic dysfunction (Feldman et al.,
12 2000). Therefore, severe inflammation may play a key role in cardiac injury and dysfunction
13 (Chen et al., 2020). In support of this, there is a severe inflammatory response in 5% of COVID-
14 19 patients associated with septic shock (Wu and McGoogan, 2020). Due to the septic shock
15 and drop in blood pressure, approximately 30% of hospitalized patients with COVID-19 require
16 vasopressors to improve blood pressure (Goyal et al., 2020). Mediating these responses in
17 some patients is a cytokine storm of similar magnitude to that induced by CAR-T cell-associated
18 cytokine storms (Del Valle et al., 2020). Additionally, severe COVID-19 is associated with sepsis
19 and bacterial products in the serum (Arunachalam et al., 2020), which are known drivers of
20 cardiac pathology and dysfunction. Cardiac dysfunction may also result in further exacerbation
21 of infectious diseases, via inadequate organ perfusion and/or immune cell infiltration. Thus,
22 preventing cytokine-induced cardiac dysfunction may potentially limit severe outcomes in
23 inflammatory diseases. However, targeted treatment strategies, particularly in severe infections
24 such as COVID-19, are currently lacking.

25 Several anti-inflammatory agents have shown clinical benefit for the acute management of
26 COVID-19. Dexamethasone improved 28-day mortality in COVID-19 patients receiving invasive
27 mechanical ventilation or oxygen at randomization (Horby et al., 2020). However, systemic
28 immunosuppression may impede viral clearance thus potentially exacerbating disease
29 (Mangalmurti and Hunter, 2020). To circumvent this, we aimed to identify cardiac-specific
30 inflammatory targets that trigger cardiac dysfunction in response to the cytokine storm,
31 reasoning that these might provide a safe and effective therapeutic option.

32 Here, we utilize multi-cellular human pluripotent stem cell (hPSC)-derived cardiac organoids
33 (hCO) combined with phosphoproteomics and single nuclei RNA-sequencing (RNA-seq) to
34 identify therapeutic targets and treatments for cardiac dysfunction. We recently adapted our
35 hCO system (Mills et al., 2019; Mills et al., 2017a) to include co-culture with endothelial cells
36 that form enhanced branched endothelial structures surrounded by pericytes (**Figure S1A**,
37 Voges et al., In Revision). This protocol results in a complex mixture of self-organising cells
38 including epicardial, fibroblasts/pericytes, endothelial cells and cardiomyocytes. This was
39 combined together with an optimized culture environment that reflects a maturation stage;
40 mimicking the postnatal metabolic environment (Mills et al., 2019; Mills et al., 2017a) followed
41 by reversion to a more adult metabolic substrate provision (see **Methods**). This platform
42 enabled rapid screening of cytokine combinations that recapitulate the COVID-19-induced
43 cytokine storm (Mangalmurti and Hunter, 2020) and cardiac dysfunction, with the subsequent
44 application of -omic assays and drug screening.

1 **RESULTS**

2 **Cytokine-induced cardiac dysfunction**

3 We began by examining the effects of a range of pro-inflammatory cytokines elevated in
4 COVID-19 patients (Huang et al., 2020) on cardiac function in our hCO (Mills et al., 2017a).
5 Inflammatory molecules tested were likely candidates in COVID-19 including: TNF, IL-1β, IFN-γ,
6 IL-6, IL-17A, and G-CSF, as well as pathogen-associated molecular patterns including poly(I:C)
7 to mimic dsRNA, and lipopolysaccharide (LPS) to mimic TLR4 activation and septic responses.
8 Using our RNA-seq data (Mills et al., 2017a), we identified that the receptor genes *IL1R1*,
9 *TNFRSF1A*, *TNFRSF1B*, *IFIH1*, *MYD88*, *IL6ST*, *IFNAR1*, *IL6R*, *TMEM173*, *IL17RA*, *IL17RB*,
10 *IL17RC*, *IL17RD*, *IL17RE*, *IFNGR1*, *TLR3*, and *TLR4* were expressed at similar or higher
11 abundance in our hCO compared to adult human heart (**Figure S1B**). In adult mouse hearts
12 many of these are enriched in non-myocyte populations (Quaife-Ryan et al., 2017) (**Figure
13 S1C**). We used single nuclei RNA sequencing (snRNA-seq) to assess cell specificity in our
14 enhanced hCO (Voges et al., In Revision). Mapping to human heart snRNA-seq (Tucker et al.,
15 2020) revealed the presence of pro-epicardial/epicardial cells, fibroblasts, activated
16 fibroblasts/pericytes and cardiomyocytes (**Figure S1D,E**). Some cardiomyocytes were fetal-like,
17 however there was a distinct sub-cluster that mapped adjacent to adult ventricular
18 cardiomyocytes from human hearts (Gilsbach et al., 2018) (**Figure S1F**). The cytokine/pro-
19 inflammatory receptors were expressed in the different cell types and were more highly
20 expressed in epicardial cells and fibroblasts (**Figure S1G**). We screened inflammatory factors in
21 all pair-wise combinations in hCOs with multiple functional measurements including contractile
22 force, rate, activation kinetics and relaxation kinetics (**Figure 1A**). TNF caused a reduction in
23 force, while IL-1β, IFN-γ, poly(I:C) and LPS caused diastolic dysfunction characterized by a
24 preserved contractile force but prolonged time from peak to 50% relaxation (**Figure S2A to E**).
25 A secondary full-factorial screen of TNF, IFN-γ, IL-1β, and poly(I:C), once again revealed that
26 TNF induced systolic dysfunction (**Figure 1B,D**) with a EC_{50} of 1 ng/mL at 48 hours (**Figure
27 S2F**). A combination of IL-1β, IFN-γ and poly(I:C) induced diastolic dysfunction (**Figure 1C,E**),
28 however also decreased the beating rate which may influence the kinetics of contraction
29 (**Figure S3A, Supplementary Video 1,2**). Changes in rate were not responsible for increased
30 relaxation time, as hCO paced at 1 Hz retained the severe diastolic dysfunction phenotype
31 (**Figure 1F, Supplementary Video 3,4**). Individually, IFN-γ and IL-1β caused concentration-
32 dependent diastolic dysfunction with an EC_{50} of 0.8 ng/mL at 48 hours and 3 ng/mL at 24 hours,
33 respectively, whereas poly(I:C) alone did not induce dysfunction (**Figure S2G to I**). These
34 results were confirmed in an independent hPSC line, where the combination of IFN-γ, IL-1β and
35 poly(I:C) induced the most consistent, robust diastolic dysfunction (**Figure S3A to E**). Taken
36 together, TNF induces systolic dysfunction consistent with previous *in vitro* (Vasudevan et al.,
37 2013) and *in vivo* (Kubota et al., 1997) studies, and the combination of IFN-γ, IL-1β and
38 poly(I:C) induces severe diastolic dysfunction in hCO. The dominant factor identified that causes
39 diastolic dysfunction, IFN-γ (**Figure S3C**), is generally elevated in heart failure patients but with
40 contradictory effects in animal models (Levick and Goldspink, 2014).

41 **Mechanisms driving cardiac cytokine storm-induced dysfunction**

42 The most common types of cardiac dysfunction observed in hospitalized COVID-19 patients are
43 right ventricular dysfunction or left ventricular diastolic dysfunction (Szekely et al., 2020).
44 Therefore, we focussed on diastolic dysfunction induced by IFN-γ, IL-1β and poly(I:C), we refer

to as 'cardiac cytokine storm' (CS). Protein phosphorylation is linked with all biological functions (Needham et al., 2019), and thus we measured the global phosphoproteome in hCO. Leveraging our latest phosphoproteomics technology (Humphrey et al., 2015; Humphrey et al., 2018), we identified over 7,000 phosphosites in each sample. We accurately pinpointed 7,927 phosphorylation sites to a single amino acid residue on ~3,000 different phosphoproteins from single-run measurements (**Figure 2A**). Preliminary studies on TNF treated hCO identified several known effects including decreased phosphorylation of protein kinase A and increased phosphorylation of beta-adrenergic receptor kinase 1 (also known as GRK2), supporting our approach (data not shown). CS treatment induced 91 phosphosites that were consistently elevated (**Figure 2B**). These sites were enriched for transcriptional responses with 35 sites found on transcription factors or chromatin-binding proteins and 13 associated with the biological process term 'cell proliferation' (FDR < 0.05, Fisher's exact test). Among these was phosphorylation of signal transducer and activator of transcription 1 (STAT1) S727 (median 13.9 fold), as well as two sites on BRD4 (Bromodomain-containing protein 4) S469 and S1083 (median 7.4 and 12.3 fold respectively) (**Figure 2B,C**). In light of the availability of specific small molecule inhibitors for each of these targets or their upstream regulators, we focused on these proteins in subsequent functional assays.

We assessed activation of individual cell populations in hCOs using snRNA-seq (**Figure 3A**) with mapping as described above (CTRL - **Figure S1D,E** and CS - **Figure S4A,B**). In the CS condition there was an increase in fibroblast and activated fibroblast number (**Figure 3B**). KEGG pathway analysis revealed a transcriptional response dominated by a viral response in both cardiomyocytes (CM1, CM2 and CM3 pooled) and fibroblasts (epicardial/fibroblast and perictye/activated fibroblasts) (**Figure 3C,D**). There were fewer downregulated genes, which were predominantly in the fibroblasts and dominated by extracellular matrix (ECM) genes including *COL1A1*, *COL3A1* and *COL4A5* (**Figure 3E**). The top predicted mediators of the transcriptional response were STAT1 and general epigenetic activation by EP300 (**Figure 3F**). This is consistent with our phosphoproteomic data (**Figure 2**), given EP300 has been shown to share upto 78% of DNA binding regions with BRD4 in chromatin immunprecipitation studies (Williams et al., 2020). These analyses together revealed a robust viral response in the heart in multiple cell populations (**Figure 3G,H**), predicted to be mediated via STAT1 and epigenetic activation including BRD4.

Drugs for the prevention and treatment of cardiac dysfunction

We next screened drugs that could potentially treat cardiac dysfunction caused by either TNF-induced systolic dysfunction or CS-driven diastolic dysfunction (**Figure 4A**). TNF is known to induce systolic dysfunction via GRK2 mediated repression of β-adrenergic receptor signaling (Vasudevan et al., 2013). The selective serotonin reuptake inhibitor, paroxetine hydrochloride, can inhibit GRK2 (Schumacher et al., 2015), but we found that it was toxic at effective *in vitro* concentrations (Guo et al., 2017) (**Figure S5A,B**). GRK2 promotes clathrin-mediated endocytosis (Evron et al., 2012), and baricitinib was recently identified as a potential AP2-associated protein kinase 1 (AAK1)-mediated endocytosis inhibitor using machine learning (Richardson et al., 2020). Baricitinib prevented TNF-induced dysfunction in hCO (**Figure 4B** and **Figure S5A,B**). However, baricitinib was only protective against TNF-induced systolic dysfunction when co-administered with TNF and was not effective after 24 h TNF treatment (**Figure 4C**). Additionally, hCO did not recover quickly from TNF-induced systolic dysfunction after the removal of TNF (**Figure 4C**) indicating that secondary remodeling events may have occurred.

1   A key signature of diastolic dysfunction under CS conditions was the elevated phosphorylation
2   of transcriptional regulators. STAT1-S727 (**Figure 2C**) is associated with assembly into
3   chromatin and is required for STAT1 transcriptional and biological activity in response to IFN-γ
4   (Sadzak et al., 2008). The putative STAT1-S727 kinase is CDK8 (Bancerek et al., 2013), so we
5   next tested two CDK8 inhibitors SEL120-34A (Rzymski et al., 2017) and BI-1347 (Hofmann et
6   al., 2020) previously shown to reduce STAT1-S727 phosphorylation. We also tested two
7   inhibitors of the JAK/STAT pathway, baricitinib and ruxolitinib. However, none of these
8   compounds, nor a broader spectrum CDK inhibitor flavopiridol, prevented the CS-induced
9   diastolic dysfunction, noting that flavipiridol was toxic and reduced force and hence all kinetic
10 parameters (**Figure S6A to H**). Notably, SEL120-34A and BI-1347 specifically attenuated the
11 rate and activation time defects under CS conditions (**Figure S6B,C,F,G**), which we validated in
12 additional experiments (**Figure S5C to F**) and may still have clinical utility in this setting.

13 We observed elevated phosphorylation of the epigenetic regulator BRD4 and other epigenetic
14 regulators in our CS treated hCO phosphoproteome, consistent with our snRNA-seq analysis.
15 We have previously shown that bromodomain extraterminal inhibitors (BETi) reduce relaxation
16 time in immature hCO (Mills et al., 2019), so we next evaluated three BETi available in an FDA
17 compound library INCB054329 (Stubbs et al., 2019), JQ-1 (Filippakopoulos et al., 2010), and
18 ABBV-744 (Faivre et al., 2020). Strikingly, INCB054329 prevented CS-induced diastolic
19 dysfunction in a dose-dependent manner (**Figure 4D, Figure S5G**) without affecting force or
20 rate (**Figure S6A to H, Supplementary Video 5**). JQ-1 also showed improved diastolic function
21 in one hPSC line at the highest concentration (**Figure S6H**), so an additional higher
22 concentration for both JQ-1 and ABBV-744 were tested. JQ-1 protected hCO against CS-
23 induced diastolic dysfunction, although INCB054329 was the most efficacious (**Figure S5H,I**). In
24 contrast, ABBV-744 increased diastolic dysfunction in the hCO, potentially via its dual actions as
25 an androgen receptor inhibitor, which is associated with prolonged QTc in patients undergoing
26 androgen deprivation therapy (Gagliano-Jucá et al., 2018). To validate BRD4 as a target we
27 used adeno associated virus 6 (AAV6) mediated delivery of shRNA and demonstrated that
28 ~74% knockdown could also reduce diastolic dysfunction in CS treated hCO (**Figure S5K**).

29 INCB054329-mediated BETi rescued dysfunctional hCO, and restored diastolic function
30 following 24 h of CS conditions (**Figure 4E**). This is potentially because CS-induced diastolic
31 dysfunction is reversible and is driven by the presence of the inflammatory mediators,
32 demonstrated by partial hCO recovery 24 h after removing CS factors (**Figure 4E**). In patients,
33 all inflammatory factors may be present simultaneously, and we found that INCB054329
34 attenuated diastolic dysfunction with all four dysfunction inducing factors, TNF, IFN-γ, IL-1β, and
35 poly(I:C), present (**Figure S5J**). Taken together CS mediates diastolic dysfunction via BRD4-
36 dependent mechanisms that can be blocked using BETi. As BRD4 is broadly expressed in our
37 hCO (**Figure 4F**), it may also be responsible for the multi-cellular response observed.

38 **INCB054329 reduces the host response to SARS-CoV-2 infection in K18-hACE2 mouse**
39 **hearts**

40 We next assessed the response to SARS-CoV-2 infection *in vivo*. As mice are not susceptible to
41 SARS-CoV-2 infection, we used a recently described K18-hACE2 model (Oladunni et al., 2020)
42 to study the response and effects of BETi (**Figure 5A**). SARS-CoV-2 infected mice had severe
43 lung pathology and substantial viral RNA reads in the lungs at 4-5 days post infection.
44 confirming successful lung infection (**Figure 5B,C**). RNA-seq of the lungs revealed increased
45 expression of 419 genes (**Figure 5D**), strongly associated with a viral response (**Figure 5E,**
46 **Table S1A**). Concordant with our hCO data, Stat1 and Ep300 were top predicted transcriptional
47 regulators (**Figure 5F, Table S1B**). Interestingly, there was only negligible infection of the heart

1 (**Figure 5C**) and no obvious pathology including necrosis, immune cell infiltration or fibrosis
2 (**Figure 5G**). However, there was a substantial and robust upregulation of a viral response in
3 the heart with ECM repression (**Figure 5H,I, Table S1A**) including *Col1a1*, *Col3a1* and *Col4a2*.
4 This was again enriched for Stat1 and Ep300 as top predicted transcriptional regulators (**Figure**
5 **5J, Table S1B**), indicating a robust systemic response in the hearts of SARS-CoV-2 infected
6 mice. This response could be partially blocked by INCB054329 treatment with repression of 91
7 genes that were enriched for the viral response (**Figure 5K to M, Table S1A**). This response
8 was more specfic to the heart, as INCB054329 did not regulate any genes in the lungs (data not
9 shown). The repression by INCB054329 was predicted to be primarily mediated via Ep300
10 rather than Stat1 (**Figure 5N, Table S1B**). These results were further supported by Ingenuity
11 Pathway Analysis of upstream regulators revealing strong activation signatures for IFNG, poly
12 rI:rC-RNA and Stat1 in both lungs and hearts of K18-hACE2 SARS-CoV-2 infected mice, which
13 INCB054329 strongly inhibited (**Table S1C**).

14 Potentially important mediators and markers of the response were found by integrating the
15 multiple datasets. The CS induced response in the hCO (either fibroblasts or cardiomyocytes)
16 and hearts of SARS-CoV-2 infected K18-hACE2 mice shared 32 regulated genes (**Figure 5O**)
17 which were enriched for the viral response (**Figure 5P**). The consistent transcriptional program
18 in CS treated hCO (both fibroblasts and cardiomyocytes) and SARS-CoV-2 infected K18-hACE2
19 mice, that were also down-regulated genes by INCB054329 treatment *in vivo* revaled 5 key
20 targets. These comprise the key inflammatory genes *Nmi*, *Tap1*, *B2m*, *Stat1* and *Lgals3bp*
21 (**Figure 5Q**). Of particular interest is LGALS3BP (galectin-3 binding protein) as it has been
22 shown to be a top-predictor of COVID-19 severity in humans (Messner et al., 2020) and
23 therefore interrogated its expression in our subsequent models.

24 **INCB054329 protects against inflammatory mediated dysfunction *in vivo* and by COVID-**
25 **19 serum**

26 The study into the efficacy of SARS-CoV-2-related cytokine storm therapeutics on the heart *in*
27 *vivo* is technically challenging in biosafety level 3 and because the severe lung/brain infection in
28 K18-hACE2 mice causes a rapid decrease in weight and requires euthanasia (**Figure 5R**). We
29 therefore used surrogate models.

30 We used a LPS-induced cytokine storm mouse model (**Figure 6A**). LPS induced pro-
31 inflammatory cytokines TNF, IL-1β and IFN-γ, which were elevated in the plasma (**Figure 6B**)
32 along with *Lgals3bp* in the heart (**Figure 6C**). Treatment with INCB054329 blocked the LPS-
33 induced pro-inflammatory cytokine production (**Figure 6B**) and *Lgals3bp* induction in the heart
34 (**Figure 6C**). We observed a marked improvement in mortality, whereby all INCB054329-treated
35 mice survived after 24 h of the LPS-challenge, compared with only 25% in the control group
36 (**Figure 6D**). To determine whether BETi could treat an established LPS-induced cytokine
37 storm, we delayed injection of INCB054329 1.5 h after LPS injection and assessed cardiac
38 function at 6 h (**Figure 6E**). INCB054329 fully prevented the decrease in cardiac function
39 observed after LPS injection (**Figure 6F**). Together these findings demonstrate that BETi using
40 INCB054329 has robust effects in preventing inflammatory-induced cardiac dysfunction *in vivo*.

41 The factors present in COVID-19 patient serum are more complex than our CS conditions. So
42 we assessed the impact of this serum on hCO (**Figure 6G, Table S2A,B**). Our most potent CS
43 factor, IFN-γ, correlates with COVID-19 disease progression and is elevated in patient serum in
44 one of the most comprehensive profiling studies to date (Ren et al., 2021). We found that IFN-γ,
45 was higher in patients with elevated BNP as a marker of cardiac stress (> 0.3 ng/ml) but not
46 CTNI as a marker of acute injury (> 0.5 ng/ml) (**Figure 6H,I**). Factors in human serum can alter
47 hCO function, as patients receiving noradrenaline as inotropic support had elevated contractile

force in hCO (**Figure 6J**). Diastolic dysfunction was induced in hCO by serum with elevated BNP (**Figure 6J**) with no viral infection detected (data not shown) and INCB054329 could prevent this response (**Figure 6K**). We also found that *LGALS3BP* induction could be prevented by treatment with multiple BETi (**Figure 6L**).

Collectively, these data indicate that BET inhibition with INCB054329 prevents cardiac dysfunction in multiple complex inflammatory models, as well as repressing the key COVID-19 severity marker LGALS3BP.

INCB054329 decreases hACE2 expression and reduces SARS-CoV-2 in hPSC-cardiac cells

SARS-CoV-2 potentially infects human hearts and has been shown to infect human pluripotent stem cell-derived cardiac cells (hPSC-CM) (Sharma et al., 2020). Recently other investigators have also demonstrated that BETi reduced Ace2 *in vivo* and SARS-CoV-2 infection (Qiao et al., 2021). So we sought to determine whether BETi blocked infection (**Figure S7A**).

We confirmed previous findings using 2D cultured hPSC-cardiac cell infection studies, where increasing the MOI increased the degree of cell death (**Figure S7B**). Infection with a low MOI (0.01) was sufficient for viral replication and cell death over 7 days (**Figure S7C**). A 3 day pre-incubation of INCB054329 was sufficient to reduce ACE2 expression ~4 fold (**Figure S7D**). Consequently, pre-treatment with INCB054329 reduced SARS-CoV-2 N protein expression (**Figure S7E**) and intracellular viral RNA (**Figure S7F**). In addition to INCB054329, the widely used BETi JQ-1 reduced SARS-CoV-2 RNA (**Figure S7G**). In our SARS-CoV-2 K-18 mouse infection studies INCB054329 treatment reduced endogenous *Ace2* in hearts *in vivo* (**Figure S7H**). Thus, BETi also has potential to block SARS-CoV-2 infection of cardiac cells in addition to preventing dysfunction.

BETi for translation to the clinic

We assessed the ability of all commercially available BETi compounds to prevent CS-induced diastolic dysfunction in hCO. We found that all compounds prevented dysfunction except for ABBV-744 (**Figure 7A**). As BETi with dual bromodomain 1 (BD1) and bromodomain 2 (BD2) activities display side-effects (Gilan et al., 2020), it is critical that we determine selectivity of the response. BD2-selective drugs such as ABBV-744 and apabetalone have limited side effects. Apabetalone has been used for up to 3 years in >1,700 humans at risk of cardiac disease with efficacy in preventing heart failure and favourable safety profile (Nicholls et al., 2021; Ray et al., 2020). ABBV-744 elevated diastolic dysfunction (**Figure 7A**), and we suspect its lack of efficacy was due to its on-target inhibition of the androgen receptor (AR). BD2-specific efficacy was confirmed using a BD2-specific molecule, RXV-2157 (**Figure 7B**) and we also confirmed efficacy with the BD-2 selective apabetalone (**Figure 7A,B**). Additionally, analysis of plasma from the ASSURE phase IIb clinical trial indicated that BD2-selective apabetalone reduced LGALS3BP in patients with cardiovascular disease (**Figure 7C**), which is a marker of COVID-19 severity (Messner et al., 2020).

We confirmed the BD2-specificity of blocking SARS-CoV-2 infection. The BD2-specific RXV-2157 and BD2-selective apabetalone molecules downregulated hACE2 (**Figure 7D**), which led to decreased surface expression (**Figure S7I**) and SARS-CoV-2 spike protein binding (**Figure S7J**). These compounds also reduced SARS-CoV-2 loading (**Figure S7K**, **Figure 7E,F**) and viral titre, including a 2.6 fold decrease in viral titre with apabetalone (**Figure 7G**).

1   Together, this demonstrates that BD2 -selective BETi drugs are lead candidates for rapid
2   clinical translation to prevent COVID-19 injury in the heart.

1 **DISCUSSION**

2 We define CS conditions resulting in severe diastolic dysfunction with 20-50% increases in time
3 to 50% relaxation in hCO. This is consistent with ~13-18% increases in cardiomyocytes derived
4 from patients with heart failure with preserved ejection fraction (HFpEF), similar absolute
5 increases of 100-150 ms (Runte et al., 2017). It is also consistent with diastolic dysfunction
6 reported in COVID-19 patients (Szekely et al., 2020), indicating our hCO model recapitulates
7 key clinical features of diastolic dysfunction.

8 Our transcriptional profiling revealed a striking similarity between the inflammatory response in
9 CS treated hCO and hearts of SARS-CoV-2 infected K18-hACE2 mice. CS also elicited a more
10 pronounced transcriptional response in the fibroblasts within hCO (**Figure 3C,D**). This was with
11 negligible viral infection in our models, meaning that inter-organ and intra-organ signalling
12 appears to play a key role in inflammation-induced cardiac dysfunction. It will be important to
13 decipher the systemic and intra-organ drivers of dysfunction also in other oragns, because
14 COVID-19 and many other inflammatory diseases can result in multi-organ dysfunction.

15 Our data establish BET inhibition as a viable therapeutic strategy to attenuate cytokine storm-
16 induced cardiac dysfunction. Previously, BETi compounds have shown efficacy in small animal
17 cytokine storm models (Nicodeme et al., 2010). There is also compelling evidence implicating
18 bromdodomain proteins as key mediators in pathological pro-fibrotic signaling in heart failure
19 (Duan et al., 2017; Stratton et al., 2019), in experimental models of pressure overload and
20 myocardial infarction–induced HF (Anand et al., 2013) and in genetic cardiomyopathies (Antolic
21 et al., 2020; Auguste et al., 2020). However, this study is instrumental in establishing BET
22 inhibition as a therapeutic intervention to prevent cardiac dysfunction caused by inflammation.

23 Clinical data from COVID-19 patients also point to additional cardiac pathologies. Microthrombi
24 were reported in the hearts of 14 out of 40 patients (35%) that died from COVID-19, which was
25 associated with areas of myocardial necrosis (Pellegrini et al., 2021). Consistent with these
26 observations, we observed that "complement and coagulation cascades" were enriched in the
27 lungs of K18-hACE2 mice with SARS-CoV-2 infection (**Figure 5E** and **Table S1**), and were
28 likely related to the viral-induced inflammatory response. Intriguingly, we identified *serpine1*
29 (also known as plasminogen activator inhibitor 1), was upregulated both in the lungs (3.9 fold)
30 and in the heart (2.8 fold, both FDR < 0.05) of SARS-CoV-2 infected K18-hACE2 mice, which
31 was abrogated in the heart upon treatment with the BETi INCB054329 (FDR < 0.05). *Serpine 1*
32 is a key inhibitor of tissue-type plasminogen activator and urokinase-type plasminogen activator,
33 and is required for fibrinolysis down-regulation and degradation of blood clots. In addition,
34 arrhythmic events have been widely reported in COVID-19 patients (Nishiga et al., 2020).
35 Indeed, we observed that arrhythmic events increased in hCO with CS, for which INCB054329
36 also conferred protection (**Figure S5L to N**). These data suggest that BET inhibition may be
37 effective in attenuating multiple deleterious aspects of systemic inflammation on the heart that
38 warrant further investigation.

39 We demonstrated that BETi are attractive therapeutic candidates, however the side effect
40 profiles of some BETi may preclude their use in the clinic. Genetic ablation studies have shown
41 that BRD4 plays an integral homeostatic role in cardiomyocytes, suggesting that the loss of BET
42 proteins may have detrimental effects on mitochondrial energy production (Kim et al., 2020;
43 Padmanabhan et al., 2020). Emerging evidence dissecting the roles of BD1 and BD2
44 bromodomains in inflammatory disease models has indicated that BD2-selective inhibition
45 preferentially blocks the induction of gene expression while minimally affecting established
46 transcription programs (Gilan et al., 2020). More recently, BD2-selective drugs such as ABBV-
47 744 and apabetalone have been developed to overcome these side-effect profiles. Whilst
48 ABBV-744 was not effective in our hCO model (potentially due to its targeting of AR), we

10

demonstrate that BD-2 selective compounds, RXV-2157 and apabetalone demonstrate efficacy. This underscores the need for careful BETi selection, despite broad ability to modulate critical target genes (**Figure 6L**) and utility for a variety of clinical conditions (Cochran et al., 2019). Importantly, BD2-selective BETi apabetalone reduced CS-induced diastolic dysfunction and downregulated ACE2 and reduced viral infection (**Figure 7**). Taken together, the efficacy and known safety profile of apabetalone make it a prime candidate to protect against cardiac injury for inflammatory diseases such as COVID-19.

The overlap in risk factors for HFpEF and COVID-19 mortality suggests that our findings may also have broader implications. HFpEF risk factors including diabetes and obesity are also associated with chronic inflammation. Recent studies have shown that elevated inflammatory markers are associated with worsening heart function in HFpEF (Sanders-van Wijk et al., 2020), thus indicating that inflammation may drive dysfunction across multiple cardiac diseases and that BET inhibitors are putative therapeutic candidates.

Limitations of the Study

Human COVID-19 patient serum and CS directly impacted hCO function. There is evidence that the heart can be inflamed in patients with COVID-19 (Kotecha et al., 2021; Puntmann et al., 2020), but whether direct cardiac inflammation is required for functional impact or whether the systemic environment is a driver of cardiac dysfunction remain to be determined. Also, larger studies are required to ascertain the full extent of the inflammatory effects on heart function in the clinic, in particular on diastolic function as found in some echocardiography studies (Szekely et al., 2020). It will be important to determine whether cardiac inflammation and cardiac function effects (which may be sub-clinical in cases) are prolonged following acute infection and whether this pre-disposes patients to future risk of cardiovascular events.

Our hCO model is free from an active immune system and the secondary effects of neurohormonal compensation present *in vivo*. Our hCO work, the lack of response in the lungs of INCB054329 treated SARS-CoV-2 infected K18-hACE2 mice and improvement of heart function with delayed INCB054329 treatment in the LPS treated mice (**Figure 6F**); all indicate robust cardiac specific effects. However, BETi within an *in vivo* setting may also reduce immune responses and cytokine induction (eg. **Figure 6B**), thus, we cannot rule this out as a potential mechanism for cardiac protection in mouse studies. In order to elucidate cardiac specific effects, genetic studies may be useful. However, these may be difficult because 1) BRD4 knockout has different effects to small molecule inhibitors (Kim et al., 2020; Padmanabhan et al., 2020) and 2) BETi drugs bind multiple BRD family members, which may be more potent that targeting one member (Gilan et al., 2020). Therefore, further mechanistic insight into the key transcriptional targets of BET proteins is important. These targets could then be manipulated using cardiac specific-genetic approaches to validate cardiac specificity of BETi. However, the feasibility of this approach will be dependent on the number of targets that are critical for BETi efficacy, as multiple targets may require genetic manipulation simultaneously.

ACKNOWLEDGEMENTS

AUTHOR CONTRIBUTIONS

R.J.M., S.J.H., G.A.Q-R., S.K., M.L., L.T.R., R.R., K.A.S., B.W.C.T., D.J.R., T.L., S.R.F., W.Z., L.L., C.M-K., D.A-B., K.K., T.B., J.E.H., investigation, L.D., H.K.V.,L.T.R., E.M., methodology, R.J.M., S.J.H., P.R.J.F., G.A.Q-R., M.L., N.R.M., D.G., L.F., E.K., R.L.J., T.D., C.B., B.G., D.T., R.R., K.S., E.R.P., T.B., J.E.H., formal analysis, J.M., C.H., D.G., L.F., S.J.N., J.J., M.S., N.C.W.W., E.K., resources, R.J.M., S.J.H., M.J.S., C.R.E., K.P.A.MD., D.G., E.K., T.B., D.A.E, K.S., A.S., D.E.J, J.E.H, conceptualization, R.J.M., S.J.H., M.J.S., C.R.E., K.P.A.MD., D.G., L.F., E.K., R.R., K.S., E.R.P., A.S., T.B., D.E.J, J.E.H, supervision, R.J.M., S.J.H., D.E.J, J.E.H. writing - original draft, all authors writing – reviewing and editing.

DECLARATION OF INTERESTS

R.J.M., J.E.H., G.A.Q.-R., D.M.T. and E.R.P. co-inventors on patents relating to cardiac organoid maturation and cardiac therapeutics. J.E.H. co-inventor on licensed patents for engineered heart muscle. R.J.M, E.R.P., D.M.T., B.G. and J.E.H. co-founders, scientific advisors and stockholders in Dynomics Inc. D.M.T. and B.G. employees of Dynomics. C.H., D.G., L.F., J.J., M.S., N.C.W.W. and E.K. employees of Resverlogix. S.J.N. honoraria and research support from Resverlogix. QIMR Berghofer Medical Research Institute filed a patent on the use of BETi.

1 **Figure 1: Identification of pro-inflammatory factors driving cardiac dysfunction.**

2 A) Schematic of experiments. Mean of n = 1,100 human cardiac organoids from 9
3   experiments.
4 B) Impact of inflammatory modulators on force (systolic function).
5 C) Impact of inflammatory modulators on time to 50% relaxation (diastolic function). n= 3-5
6   human cardiac organoids from 1 experiment.
7 D) TNF causes systolic dysfunction. n = 37 and 63 human cardiac organoids for CTRL and
8   TNF conditions, respectively from 6 experiments.
9 E) Cardiac cytokine storm (CS) causes diastolic dysfunction n = 49 and 73 human cardiac
10   organoids for CTRL and CS conditions, respectively from 6 experiments.
11 F) Representative force curve of human cardiac organoids under CTRL and cardiac
12   cytokine storm (CS) conditions (1 Hz) 48 h after treatment. Time to 50% relaxation under
13   paced conditions (1 Hz) 48 h after treatment. n = 15 and 17 human cardiac organoids
14   from 3 experiments.

15 Data presented as mean ± SEM. Cardiac cytokine storm (CS): IL-1β, IFN-γ and poly(I:C). Ta
16 – time from 50% activation to peak, Tr – time from peak to 50% relaxation. Human
17 pluripotent stem cell (hPSC)-derived cardiac cells- AA line (B,C) and HES3 line (D-F).
18 Endothelial cells- RM3.5 line (B,C) and RM3.5 or CC lines (D-F). Bold outline indicates p
19 <0.05 using a one-way ANOVA with Dunnett's multiple comparisons test comparing each
20 condition to CTRL at the respective time points (B,C). ** p<0.01, *** p<0.001, **** p<0.0001,
21 using Student's t-test (D-E). See additional functional data in **Figures S1 to 3**. Inflammatory
22 screen in B-E repeated in an additional cell line in **Figure S3**.
23

1 **Figure 2: Phosphoproteomics reveals signaling driving cardiac dysfunction.**

2   A) Schematic of the experiment.
3   B) Enriched phosphopeptides in human cardiac organoids following cardiac cytokine storm
4   (CS) treatment after 1 h. TF/TA circles depict transcription factors and transcriptional
5   activators.
6   C) Phosphorylation sites induced by CS on STAT1 and BRD4 proteins.

7 CS - cardiac cytokine storm. Human pluripotent stem cell-derived cardiac cells- AA line.
8 Endothelial cells- RM3.5 line.
9

14

1 **Figure 3: Single nuclei RNA-sequencing reveals cardiac cytokine storm activates viral**
2 **responses in human cardiac organoids**
3   A) Schematic of experiment.
4   B) Cell compositions identified in single nuclei RNA-sequencing.
5   C) Differential normalized log2 expression in cardiomyocytes and fibroblasts following
6   cardiac cytokine storm treatment (all populations pooled for each cell type).
7   D) Activation of viral responses in cardiomyocytes and fibroblasts revealed using KEGG
8   pathway analysis of upregulated genes. Size represents number of genes regulated and
9   the pathways of the coloured circles are highlighted by the text.
10   E) Repression of extracellular matrix processes in fibroblasts revealed using KEGG
11   pathway analysis of down-regulated genes. Size represents number of genes regulated
12   and the pathways of the coloured circles are highlighted by the text.
13   F) STAT1 and EP300 are predicted as key transcriptional mediators. Values presented are
14   adjusted P values, number of genes regulated by the transcription factor/number of
15   genes regulated, and % of genes regulated over the total. The size of the coloured slices
16   represent the fraction of genes regulated (180° = 100%), and overlaps for each
17   transcription factor are also depicted.
18   G) Key upregulated genes (see **Figure 5Q**) in cardiac cytokine storm treated human
19   cardiac organoids.
20   H) UMAP of CTRL and cardiac cytokine storm treated human cardiac organoid
21   subpopulations and expression of key regulated genes.

22 hCO – human cardiac organoid. CM – cardiomyocyte, Prlf – proliferating, EpC – epicardial cells,
23 Fib – fibroblasts, Per – pericytes, Afib – activated fibroblasts. Human pluripotent stem cell-
24 derived cardiac cells- HES3 line. Endothelial cells- RM3.5 line. See additional data in **Figure**
25 **S4**.

26

1 **Figure 4: Discovery of drugs that improve cardiac function.**

2 A) Schematic of experiment.
3 B) Protection against systolic dysfunction (force of contraction) by baricitinib. n = 9-32
4   human cardiac organoids from 2-3 experiments.
5 C) Assessment of human cardiac organoid recovery from TNF and baricitinib treatment. n =
6   6-12 human cardiac organoids from 1-2 experiments.
7 D) Protection against diastolic dysfunction (time to 50% relaxation time) by INCB054329. n
8   = 8-43 human cardiac organoids from 2-4 experiments.
9 E) Assessment of human cardiac organoid recovery from cardiac cytokine storm and
10   INCB054329 treatment. n = 6-11 human cardiac organoids from 1-2 experiments.
11 F) BRD4 is expressed in all cell populations in human cardiac organoids.

12 CS – cardiac cytokine storm. Data presented as mean ± SEM. Human pluripotent stem cell-
13 derived cardiac cells- HES3. Endothelial cells- RM3.5. *p<0.05, *** p<0.001, **** p<0.0001
14 using one-way ANOVA with Dunnett's multiple comparisons test compared to TNF (B) or
15 compared to cardiac cytokine storm (D). # p<0.05 compared to CTRL at the same time-
16 point, and * p<0.05 compared to specific condition at 0 h with colour indicating comparison,
17 using two-way ANOVA with Dunnett's multiple comparisons test compared to CTRL (C,E).
18 Drug screening was confirmed across in an additional cell line and additional data is in
19 provided in **Figure S5 and 6**.

20

Figure 5: SARS-CoV-2 activates viral responses in the heart repressed by INCB054329.

A) Schematic of the experiment.

B) Lungs of SARS-CoV-2 infected K18-hACE2 mice 5 days post infection. Infection causes sloughing of bronchial epithelium, and white arrowheads show (A) collapse of alveolar spaces and (B) bronchiolar lumen.

C) Severe lung infection with no/negligible heart infection at 4 days post infection. n = 5 mice per group.

D) Lung RNA-sequencing reveals a robust upregulation (logFC > 0.5) of 419 genes and downregulation (logFC < -0.5) of 98 genes, both FDR < 0.05. n = 5 mice per group.

E) Activation of viral responses in lungs revealed using KEGG pathway analysis of upregulated genes. Size represents number of genes regulated and the pathways of the coloured circles are highlighted by the text.

F) Stat1 and Ep300 are predicted as key transcriptional mediators of infection in the lungs.

G) Hearts of SARS-CoV-2 infected K18-hACE2 mice 5 days post infection. Relatively normal, with no significant necrosis, fibrosis (Masson's Tri-chrome not shown) or immune infiltrates.

H) Heart RNA-sequencing reveals a robust upregulation (logFC > 0.5) of 249 and downregulation (logFC < -0.5) of 159 genes, both FDR < 0.05. n = 5 mice per group.

I) Activation of viral responses in hearts revealed and repression of ECM using KEGG pathway analysis of upregulated genes and downregulated genes. Size represents number of genes regulated and the pathways of the coloured circles are highlighted by the text.

J) Stat1 and Ep300 are predicted as key transcriptional mediators in the heart.

K) PCA of heart RNA-sequencing samples. n = 4-5.

L) Heart RNA-sequencing reveals a robust upregulation (logFC > 0.5) of 11 genes and downregulation (logFC < -0.5) of 91 genes, both FDR < 0.05 by INCB054329. n = 4-5 mice per group.

M) Repression of viral responses in hearts revealed using KEGG pathway analysis of down-regulated genes. Size represents number of genes regulated and the pathways of the coloured circles are highlighted by the text.

N) Ep300 is predicted as the key transcriptional mediator of INCB054329 effects in the heart.

O) Cross-analysis of the transcriptional responses in human cardiac organoids with hearts of SARS-CoV-2 infected K18-hACE2 mice.

P) Co-regulated genes in panel (O) reveals a consistent activation of viral responses in both models using KEGG pathway analysis of upregulated genes. Size represents number of genes regulated and the pathways of the coloured circles are highlighted by the text.

Q) Genes induced by both cardiac cytokine storm in human cardiac organoids and SARS-CoV-2 infected K18-hACE2 mouse hearts that are also repressed by INCB054329.

R) Severe weight loss by 4-5 days post infection in SARS-CoV-2 infected K-18-hACE2 mice is due to severe lung infection and also brain infection and euthanasia is required.

d.p.i. – days post infection. CS - cardiac cytokine storm. Data presented as mean ± SEM.. ** $p < 0.01$, using Mann-Whitney *** $p < 0.001$ and **** $p < 0.0001$ using two-way ANOVA with Sidak's post hoc test compared to CTRL. For D, H, L – red dots are regulated as per the described cut-offs and grey dots are not. For F,J and N - Values presented are adjusted P values, number of genes regulated by the transcription factor/number of genes regulated, and % of genes regulated over the total. The size of the coloured slices represent the fraction of genes regulated

1   (180° = 100%), and overlaps for each transcription factor are also depicted. Additional data

2   bioinformatics analysis is provided in **Table S1A to C**.

3

Figure 6: INCB054329 prevents cardiac dysfunction in a mouse lipopolysaccharide-induced cytokine storm model and in response to COVID-19 patient serum.

A) Schematic for B-D.
B) INCB054329 blocks cytokine induction 6 h after lipopolysaccharide injection. n = 5-6 mice.
C) INCB054329 blocks induction of *Lgals3bp* 6 h after lipopolysaccharide injection. n = 5-6 mice.
D) Kaplan-Meier curve of survival after lipopolysaccharide injection. n = 12 control and 11 INCB054329 treatment (67 mg/kg).
E) Schematic for F.
F) INCB054329 prevents the reduction in ejection fraction 6 h after lipopolysaccharide injection. n = 3-4 mice at 0 and 1.5 h and n= 8 at 6 h.
G) Schematic for H-K.
H) IFN-γ was not higher in patients with elevated cardiac troponin I (CTNI > 0.5 ng/ml). n = 27.
I) IFN-γ was higher in patients with elevated brain natriuretic peptide (BNP > 0.3 ng/ml). n = 27.
J) Serum from COVID-19 patients with elevated brain natriuretic peptide induce diastolic dysfunction. Orange highlights human cardiac organoids with elevated force of contraction. Blue highlights dysfunctional human cardiac organoids.
K) Diastolic dysfunction induced by COVID-19 patient 6 serum is prevented by 1 μM INCB054329. n = 4-9 human cardiac organoids from 1 experiment
L) *LGALS3BP* is induced by cardiac cytokine storm and repressed by bromodomain and extraterminal protein inhibition in human cardiac organoids. n = 3 each (2 human cardiac organoids pooled per n).

LPS – lipopolysaccharide. CS – cardiac cytokine storm. Data presented as mean ± SEM. Human pluripotent stem cell-derived cardiac cells- HES3 line. Endothelial cells- RM3.5 line. *p<0.05, **p<0.01, *** p<0.001 and **** < 0.0001, using one-way ANOVA with Tukey's multiple comparisons test (B,C) with Dunnett's multiple comparisons test compared to CTRL serum (J,K) or compared to CS (L), or using two-way ANOVA with Sidak's multiple comparisons test (F), or using Mann-Whitney (I). P-value calculated using Gehan-Breslow-Wilcoxon test (D).Additional data patient data is provided in **Table 2 S2A,B**.

1 **Figure 7: Bromodomain and extraterminal protein inhibitors targeting bromodomain 2 are**
2 **effective therapeutic candidates.**

3   A) All bromodomain and extraterminal protein inhibitors (except ABBV-744) used in clinical
4   trials prevent cardiac cytokine storm-induced diastolic dysfunction. n = 12-19 human
5   cardiac organoids from 3 experiments.
6   B) Bromodomain and extraterminal protein inhibitors specific (RVX-2157) or selective
7   (apabetalone) for bromodomain 2 prevent cardiac cytokine storm-induced diastolic
8   dysfunction. n = 12-18 hCOs from 3 experiments.
9   C) Apabetalone decreases serum LGALS3BP in the phase IIb ASSURE clinical trial. Data
10   are changes from baseline. n = 47 both groups.
11   D) Bromodomain and extraterminal protein inhibitors specific (RVX-2157) or selective
12   (apabetalone) for bromodomain 2 decrease ACE2 expression after 3 days.
13   E) Pre-treatment for 3 days with bromodomain and extraterminal protein inhibitors specific
14   (RVX-2157) or selective (apabetalone) for bromodomain 2 reduce SARS-CoV-2
15   infection. E-gene expression in 2D cultures 3 days after infection. n = 6-8 from 2
16   experiments.
17   F) Apabetalone 3 day pre-treatment to reduces SARS-CoV-2 infection. E-gene expression
18   in 2D cultures 3 days after infection. n = 6 from 1 experiment.
19   G) Apabetalone or JQ-1 3 day pre-treatment reduces SARS-CoV-2 titre in hPSC-CM 3 days
20   after infection. n = 6 from 1 experiment.

21 CS – cardiac cytokine storm. TCID50 - Fifty-percent tissue culture infective dose. Human
22 pluripotent stem cell-derived cardiac cells- HES3 line (no endothelial cells) (A-C, F, G) or HES3
23 and AA lines (E). Data presented as mean ± SEM for all plots except for C, which is median ±
24 interquartile range. * $p < 0.05$, ** $p < 0.01$, *** $p < 0.001$, **** $p < 0.0001$, using one-way ANOVA
25 with Dunnett's multiple comparisons test (A,B – CS, E,F,G - DMSO) or Mann-Whitney (C).

1   **Supplementary Figure S1: Expression of immunomodulatory receptors and signalling**
2   **mediators. Related to Figure 1.**

3   A) Whole-mount immunofluorescent images of human cardiac organoids stained with CD31
4   (endothelial cells), NG2 (pericytes), cardiac troponin T (cardiomyocytes) and
5   Hoescht33342. Scale = 50 µm.
6   B) Comparison of immunomodulatory receptors and signalling mediators in human cardiac
7   organoids relative to human adult heart using existing bulk RNA-sequencing data (n = 4
8   experiments for hCO) (Mills et al., 2017a). All were identified in human cardiac organoids
9   except CSF1R which is leukocyte specific.
10   C) Cell type specificity of immunomodulatory receptors and signalling mediators in adult
11   mouse hearts using existing bulk RNA-sequencing data (n = 4 experiments) (Quaife-
12   Ryan et al., 2017).
13   D) Normalized expression of genes in human cardiac organoids that mark the human heart
14   sub-populations defined in a recent publication (Tucker et al., 2020).
15   E) UMAP clustering of single nuclei RNA-sequencing of human cardiac organoids using the
16   enhanced protocol (Voges et al., In Preparation). Location of key markers for different
17   cell populations are also highlighted.
18   F) Principal component analysis of our single nuclei RNA-sequencing in comparison to
19   purified bulk RNA-sequencing of purified human cardiomyocyte nuclei (Gilsbach et al.,
20   2018).
21   G) Expression of immunomodulatory receptors and signalling mediators in different cell
22   populations in the human cardiac organoids.

23   Data presented as mean ± SEM. hCO – human cardiac organoids. Human pluripotent stem cell-
24   derived cardiac cells- AA line. Endothelial cells- RM3.5 line.

25

1 **Supplementary Figure S2: Screening for the impact of pro-inflammatory factors on**
2 **human cardiac organoid function. Related to Figure 1.**

3 A) Contraction force
4 B) Contraction rate
5 C) Time from 50% activation to peak
6 D) Time from peak to 50% relaxation

7 (A-D) Human cardiac organoid function normalized to baseline contraction parameters at 0
8 hr. [#] Due to a microscope camera shutter issue at the 0 h time point, IL-1β & IL-17A is
9 normalized to the 1 h time point. Bold outline indicates p <0.05 using a one-way ANOVA
10 with Dunnett's multiple comparisons test comparing each condition to CTRL at comparable
11 time point. n= 2-5 human cardiac organoids for treatments, n= 7-9 human cardiac organoids
12 for CTRL from 1 experiment. Data are presented as mean ± SEM. Human pluripotent stem
13 cell-derived cardiac cells- AA line. Endothelial cells- RM3.5 line.

14 E) Coefficients of linear regression performed using binary predictors (cytokine
15   presence/absence) with time from peak to 50% relaxation as the outcome variable at 24
16   h. Coefficients represent the mean change in the response given one unit change in the
17   predictor. Sign of the coefficient represents the direction of the change between
18   predictor and response. Overall, presence of IFN-γ, IL-1β, poly(I:C) all lead to increased
19   relaxation times whilst presence of TNF leads to a reduced relaxation. * p <0.05, **
20   p<0.01, **** p<0.0001 using regression modelling.
21 F) Dose-response curves for TNF, force of contraction
22 G) Dose-response curves for IFN-γ, time to 50% relaxation
23 H) Dose-response curves for IL-1β, time to 50% relaxation
24 I) Dose-response curves for poly(I:C), time to 50% relaxation

25 (F-I) n= 4-5 human cardiac organoids per condition per concentration from 1 experiment.
26 Data are presented as mean ± SEM. Human pluripotent stem cell-derived cardiac cells-
27 HES3 line. Endothelial cells- RM3.5 line. Dose-response curve was generated using
28 nonlinear regression (variable slope model, sigmoidal- 4 parameter logistic) to determine
29 cytokine EC_{50}.

30

31

1 **Supplementary Figure S3: Validation of pro-inflammatory factor screen in an additional**
2 **cell line and regression analysis. Related to Figure 1.**

3   A) Validation of functional inflammatory modulator screening parameters in an additional
4   cell line. n= 2-6 human cardiac organoids for treatments, n= 7 human cardiac organoids
5   for CTRL from 1 experiment.
6   B) Overall impact of inflammatory modulators on time to 50% relaxation (diastolic function)
7   at 24 h for both lines tested. n= 6-12 human cardiac organoids from 2 experiments.
8   C) Coefficients of linear regression performed (order = 2) using binary predictors (cytokine
9   presence/absence) with relaxation time as the outcome variable. Coefficients represent
10   the mean change in the response given one unit change in the predictor. Sign of the
11   coefficient represents the direction of the change between predictor and response. The
12   presence of IFN-γ, poly(I:C) and IL-1β lead to increased time to 50% relaxation.
13 D) Validation of TNF systolic dysfunction in an additional cell line. n = 23-25 from 3
14   experiments.
15 E) Validation of cardiac cytokine storm (CS) induced diastolic dysfunction in an additional
16   cell line. n = 19-20 human cardiac organoids from 3 experiments

17 Data presented as mean ± SEM. Cardiac cytokine storm (CS): IL-1β, IFN-γ and poly(I:C).
18 Human pluripotent stem cell-derived cardiac cells - HES3 (A), HES3 and AA (B) or AA (D,E)
19 lines. Endothelial cells – CC (A), RM3.5 (B), or RM3.5 and CC (D,E) lines. Bold outline indicates
20 p <0.05 using one-way ANOVA with Dunnett's multiple comparisons test comparing each
21 condition to CTRL at its' time point (A). * p <0.05, *** p<0.001, **** p<0.0001 using using one-
22 way ANOVA with Dunnett's multiple comparisons test comparing each condition to CTRL (B),
23 regression modelling (C) or Students t-test (D,E).

1   **Supplementary Figure S4: Populations in human cardiac organoids treated with cardiac**
2   **cytokine storm. Related to Figure 3.**

3   A) Normalized expression of genes in human cardiac organoids that mark the human heart
4   sub-populations defined in a recent publication (Tucker et al., 2020).
5   B) UMAP clustering of single nuclei RNA-sequencing data for cardiac cytokine storm
6   treated human cardiac organoids. Location of key markers for different cell populations
7   are also highlighted.

8

1 **Supplementary Figure S5: Drugs and targets protecting against inflammation-driven**
2 **dysfunction in human cardiac organoids. Related to Figure 4.**

3   A) Human cardiac organoids were concurrently treated with 100 ng/ml TNF and inhibitors
4   and then functionally assessed at 24 h. n = 4-6 human cardiac organoids from 1
5   experiment.
6   B) Validation in an additional cell line. Human cardiac organoids were concurrently treated
7   with 100 ng/ml TNF and inhibitors and then functionally assessed at 24 h. n = 3-23
8   human cardiac organoids from 1-2 experiments.

9   (C-F) Human cardiac organoids were concurrently treated with the cardiac cytokine storm
10   and CDK8-STAT1 S727 inhibitors, and then functionally assessed at 24 h. n = 9-21 human
11   cardiac organoids from 2 experiments.

12   C) Contraction force.
13   D) Contraction rate.
14   E) Time from 50% activation to peak.
15   F) Time to 50% relaxation.
16   G) Validation of INCB054329 protection in an additional cell line. Time to 50% relaxation.
17   Human cardiac organoids were concurrently treated with the cardiac cytokine storm and
18   INCB054329, and then functionally assessed at 24 h. n = 4-12 human cardiac organoids
19   from 1-2 experiments.
20   H) Multiple bromodomain extraterminal protein inhibition prevents cardiac cytokine storm
21   induced diastolic dysfunction, presented as change relative to increased relaxation time.
22   n = 8-43 human cardiac organoids from 2-4 experiment.
23   I) Validation of results in an additional cell line. Multiple bromodomain extraterminal protein
24   inhibition prevents cardiac cytokine storm induced diastolic dysfunction, presented as
25   change relative to increased relaxation time. n = 14-15 for CTRL and cardiac cytokine
26   storm conditions and 4-6 human cardiac organoids from 1-2 experiments.
27   J) Assessment of INCB054329 efficacy in conditions with cardiac cytokine storm with the
28   addition of TNF. n = 6-16 human cardiac organoids from 1-2 experiments.
29   K) BRD4 knockdown prevents cardiac cytokine storm induced diastolic dysfunction,
30   presented as normalized relaxation time. n = 5-8 human cardiac organoids from 1
31   experiment.
32   L) Representative force trace of a CTRL human cardiac organoid.
33   M) Representative force trace of different types of arrhythmias in human cardiac organoids
34   treated with cardiac cytokine storm.
35   N) Arrhythmic events in human cardiac organoids per experiment. n = 4-7 experiments.

36   CS – cardiac cytokine storm. Data presented as mean ± SEM. Human pluripotent stem cell-
37   derived cardiac cells- HES3 (A,C-F,H,J,K with no endothelial cells, L-N) or AA (B,G,I) lines.
38   Endothelial cells- RM3.5 (A,C-F,H,J,L-N) or CC(B,G,I) lines. * p<0.05, **, p < 0.01, ***
39   p<0.001, **** p<0.0001, using a one-way ANOVA with Dunnett's multiple comparisons test
40   compared to TNF (A,B) CS (C-I), CS + AAV6-shSCR (scramble control) (K) or with Tukey's
41   multiple comparison test (J) or with Kruskal-Wallis comparisons test to CTRL (N).

42

1 **Supplementary Figure S6: Screening for compounds that prevent cardiac cytokine storm**
2 **induced diastolic dysfunction. Related to Figure 4.**

3   A) Contraction force in human cardiac organoids.
4   B) Contraction rate in human cardiac organoids.
5   C) Time to 50% activation in human cardiac organoids.
6   D) Time to 50% relaxation in human cardiac organoids.
7   E) Contraction force in human cardiac organoids from an additional line.
8   F) Contraction rate in human cardiac organoids from an additional line.
9   G) Time to 50% activation in human cardiac organoids from an additional line.
10   H) Time to 50% relaxation in human cardiac organoids from an additional line.

11 Human cardiac organoids were concurrently treated with the cardiac cytokine storm (CS) and
12 compounds, and then functionally assessed at 24 h. (A-D) n = 4-11 and (E-F) n = 3-9 hCOs per
13 condition from 1 experiment. Data presented as mean ± SEM. Human pluripotent stem cell –
14 derived cardiac cells - HES3 (A-D) or AA (E-H) lines. Endothelial cells – RM3.5 (E-H) or CC (E-
15 H) lines. *$p<0.05$, ** $p<0.01$, *** $p<0.001$, **** $p<0.0001$, using one-way ANOVA with Dunnett's
16 multiple comparisons test compared cardiac cytokine storm.

17

18

1 **Supplementary Figure S7: Pre-treatment with INCB054329 prevents SARS-CoV-2**
2 **infection of cardiac cells. Related to Figure 7.**

3 A) Schematic of the experiments.
4 B) Optimization of loading with increasing cell death of 2D cardiac cells with increasing
5   SARS-CoV-2 infection.
6 C) Infection at low multiplicity of infection (0.01) results in viral replication and eventually
7   death following SARS-CoV-2 infection of 2D cardiac cells. n = 6 from 3 experiments.
8 D) ACE2 expression in 2D cultured cardiac cells pre-treated with 1 µM INCB054329 for 3
9   days.
10 E) Immunostaining of cardiomyocytes and SARS-CoV-2 reveals that 1 µM INCB054329
11   reduces viral loading.
12 F) Pre-treatment with 1 µM INCB054329 for 3 days reduces SARS-CoV-2 infection. E-gene
13   expression in 2D cultured cardiac cells 3 days after infection. n = 6 from 2 experiments.
14 G) Pre-treatment with 3 µM JQ-1 for 3 days reduces SARS-CoV-2 infection. E-gene
15   expression in 2D cultured cardiac cells 3 days after infection. n = 8 from 2 experiments.
16 H) INCB054329 decreases endogenous *mAce2* expression in hearts in vivo. n = 4-5 mice.
17 I) Flow cytometry analysis of ACE2 on cardiomyocytes (CD90 negative) and CD90 positive
18   stromal cells. Analysis was performed in 2 different cells lines in separate experiments.
19 J) Flow cytometry analysis of spike protein binding on cardiomyocytes (CD90 negative)
20   and CD90 positive stromal cells. Analysis was performed in 2 different cells lines in
21   separate experiments.
22 K) Immunostaining of cardiomyocytes and SARS-CoV-2 reveals that 30 µM apabetalone
23   preserves cardiomyocyte structures and reduces viral loading.

24 All scale bars = 20 µm. TCID50 - Fifty-percent tissue culture infective dose. Data presented as
25 mean ± SEM. Human pluripotent stem cell-derived cardiac cells – HES3 (C,D,K), AA (E,F) or
26 HES3 and AA (G,I,J) lines. * p<0.05, **** p<0.0001, using one-way ANOVA with Dunnett's
27 multiple comparisons test (C - compared day 0 and F,G – compared to DMSO) and Mann-
28 Whitney (H).

29

1   **STAR METHODS**

2   **RESOURCE AVAILABILITY**

3   **Lead Contact**

4   Further information and requests for resources and reagents should be directed to and will be

5   fulfilled by the lead contact, James E Hudson james.hudson@qimrberghofer.edu.au

6   **Materials Availability**

7   This study did not generate new unique reagents except for RVX-2157 for which requests
8   should be addressed to Resverlogix.

9   **Data and Code Availability**

10   Additional   Supplemental   Items   are   available   from   Mendeley   Data   at
11   doi:10.17632/xxwbsvf3ms.1. Mass spectrometry-based proteomics data have been deposited to
12   the   ProteomeXchange   Consortium   (http://proteomecentral.proteomexchange.org)   via   the
13   PRIDE partner repository (Deutsch et al., 2017) with the dataset identifier PXD020994. snRNA-
14   seq   and   bulk   RNA-seq   data   has   been   deposited   in   ENA,   accession   number:
15   EGAS00001004626 and EGAS00001004626. All Matlab m-files will be provided upon request
16   as they require custom training.

17   **EXPERIMENTAL MODEL AND SUBJECT DETAILS**

18   **Mice**

19   Mouse work was undertaken in accordance with the Australian Code for Care and Use of
20   Animals for Scientific Purposes, as outlined by the National Health and Medical Research
21   Council of Australia. Animal work was approved by the QIMR Berghofer Medical Research
22   Institute and University of Queensland Animal Ethics Committees.

23   For LPS experiments wild-type (WT) C57BL/6 were purchased from Walter and Eliza Hall
24   Institute for Medical Research, the Australian Research Centre in Western Australia or bred in
25   house at QIMR Berghofer Medical Research Institute. Mice used in this study were older than 6
26   weeks and were sex-matched. The number of mice in each group of treatment for each
27   experiment is indicated in the figure legends. No mice were excluded based on pre-established
28   criteria and randomization was applied immediately prior to treatment in therapy experiments.

29   For SARS-CoV-2 infection studies, heterozygous K18-hACE2 C57BL/6J mice (strain B6.Cg-
30   Tg(K18-ACE2)2Prlmn/J) were purchased from The Jackson Laboratory, USA, and bred in
31   house at QIMR Berghofer Medical Research Institute and genotyped using standard PCR as
32   per Jackson Labs genotyping protocol. Female mice were used for experiments.

33   **Cell lines**

34   Ethical approval for the use of human embryonic stem cells (hESCs) was obtained from QIMR
35   Berghofer's Ethics Committee and was carried out in accordance with the National Health and
36   Medical Research Council of Australia (NHMRC) regulations. hESCs utilized were female HES3
37   (WiCell). A male RM3.5 iPSC line was used (generated by Edouard Stanley (Murdoch
38   Children's Research Institute, Melbourne, Australia)). The following cell lines were obtained
39   from the CIRM hPSC Repository funded by the California Institute of Regenerative Medicine:
40   CW30382A (male, designated AA) and CW30318C (female, designated CC) which were both
41   obtained   from   FujiFilm.   hPSC   lines   were   maintained   in   mTeSR-1   (Stem   Cell
42   Technologies)/Matrigel (Millipore) and passaged using TrypLE (ThermoFisher Scientific) or
43   ReLeSR (Stem Cell Technologies). Quality control was performed with Karyotyping and
44   mycoplasma testing.

1 **Human COVID-19 plasma and serum**

2 Plasma samples were obtained from individuals with PCR confirmed COVID-19 infection in the
3 community or hospital as a part of the COVID-19 Biobank (Alfred Human Research and Ethics
4 Committee - Project 182/20). Individuals consented to provide additional blood that was
5 processed within 24 h of collection for plasma and peripheral blood mononuclear cells. Whole
6 blood was centrifuged at 1000 x g for 10 min at 22°C-24°C then plasma removed within 5 mm of
7 the buffy coat. Plasma aliquots were transferred to 2 ml cryovials for long term storage at −
8 80°C. Plasma was thawed and immediately use for ELISA for CTNI, IFN-γ and BNP. Calcium
9 was added to 10 mM to normalize calcium levels of citrated plasma and clot. The supernatant
10 was removed (serum) and used for the hCO experiments (50% serum/50% WM). No viral RNA
11 was detected in hCO treated with human COVID-19 serum.

12 **Human ASSURE trial plasma**

13 The design and rationale of the ASSURE trial (ClinicalTrials.gov identifier NCT01067820) is
14 described in. Patients with established cardiovascular disease received 200 mg apabetalone
15 daily for 26 weeks on top of standard of care, which included statins. Baseline and end of study
16 EDTA plasma samples were analysed using SOMAScan™.

17 **SARS-CoV-2 stock production and titration at QIMR Berghofer**

18 SARS-CoV-2 infection studies at QIMR Berghofer were conducted in a dedicated PC3 (BSL3)
19 suite, with safety approval from the QIMR Safety Committee (P3600). The SARS-CoV-2 virus
20 was isolated from a patient and was a kind gift from Queensland Health Forensic & Scientific
21 Services, Queensland Department of Health; the isolate, hCoV-19/Australia/QLD02/2020; has
22 been sequenced as is available at GISAID (https://www.gisaid.org/). Virus stock was generated
23 by infecting Vero E6 cells (C1008, ECACC, Wiltshire, England; Sigma Aldridge, St. Louis, MO,
24 USA) and after 3 days culture supernatant was clarified by centrifugation at 3000 x g for 15 min
25 at 4°C, and was aliquoted and stored at 80°C. Virus titre was determined using standard $TCID_{50}$
26 assay by infecting Vero E6 cells with 10-fold serial dilutions of virus stock and measuring
27 cytopathic effect with titre calculation by the method of Spearman and Karber. Virus was
28 determined to be mycoplasma free (La Linn et al., 1995) and fetal calf serum used for culture
29 determined to be endotoxin free (Johnson et al., 2005).

30 **SARS-CoV-2 stock production at The Doherty Institute**

31 SARS-CoV-2 isolate CoV/Australia/VIC01/2020, provided by the Victorian Infectious Diseases
32 Reference Laboratory (VIDRL) was amplified in Vero cells and stock vials were stored at -80°C.
33 The amplified virus was sequenced to confirm that there were no mutations resulting from
34 passage in Vero cells. All work with infectious virus was performed inside a biosafety cabinet, in
35 a biosafety containment level 3 facility, and personnel wore powered air-purifying respirators
36 (3M TR-315A VERSAFLO Cat# RPPKTR315A, from Safetyquip) or P2 masks. Vero cells were
37 obtained from VIDRL and maintained in Minimum Essential Medium (MEM, Media Preparation
38 Unit, Peter Doherty Institute) with 5% FBS, Penicillin-Streptomycin, GlutaMax (and 7.5ml
39 HEPES (all ThermoFisher Scientific).

40 **METHOD DETAILS**

41 **Cardiac differentiation**

42 Cardiac differentiation was performed as previously described (Hudson et al., 2012; Mills et al.,
43 2017a; Voges et al., 2017). hPSCs were seeded on Matrigel-coated flasks at 2×10^4 cells/cm^2
44 and cultured in mTeSR-1 for 4 days. To induce cardiac mesoderm, hPSCs were cultured in
45 RPMI B27-medium (RPMI 1640 GlutaMAX+ 2% B27 supplement without insulin, 200 μM L-
46 ascorbic   acid   2-phosphate   sesquimagnesium   salt   hydrate   (Sigma)   and   1%

1 Penicillin/Streptomycin (ThermoFisher Scientific), supplemented with 5 ng/ml BMP-4 (RnD
2 Systems), 9 ng/ml Activin A (RnD Systems), 5 ng/ml FGF-2 (RnD Systems) and 1 μM
3 CHIR99021 (Stem Cell Technologies). Mesoderm induction required daily medium exchanges
4 for 3 days. This was followed by cardiac specification using RPMI B27- containing 5 μM IWP-4
5 (Stem Cell Technologies) for another 3 days, and then further 7 days using 5 μM IWP-4 RPMI
6 B27+ (RPMI1640 Glutamax + 2% B27 supplement with insulin, 200 μM L-ascorbic acid 2-
7 phosphate sesquimagnesium salt hydrate and 1% Penicillin/Streptomycin) with media change
8 every 2-3 days. For the final 2 days of differentiation, hPSCs were cultured in RPMI B27+.
9 Harvest of differentiated cardiac cells involved enzymatic digestion, firstly in 0.2% collagenase
10 type I (Sigma) containing 20% fetal bovine serum (FBS) in PBS (with Ca^{2+} and Mg^{2+}) at 37°C for
11 1 h, and secondly in 0.25% trypsin-EDTA at 37°C for 10 minutes. Cells were filtered through a
12 100 μm mesh cell strainer (BD Biosciences), centrifuged at 300 x g for 3 min, and resuspended
13 in α-MEM Glutamax, 10% FBS, 200 μM L-ascorbic acid 2-phosphate sesquimagnesium salt
14 hydrate and 1% Penicillin/Streptomycin. Previous flow cytometry analysis indicated that
15 differentiated cardiac cells were ~70% α-actinin+/CTNT+ cardiomyocytes, ~30% CD90 stromal
16 cells (Voges et al., 2017).

17 **Endothelial differentiation**

18 Endothelial cell differentiation was performed following a protocol modified from (Orlova et al.,
19 2014). hPSCs were seeded onto Matrigel-coated T-25 or T-75 tissue culture flasks at the
20 density 5 x 10^3 cells/cm^2 and cultured in mTeSR-1 for 3 days. Mesoderm was induced with
21 RPMI B27- (RPMI 1640 GlutaMAX+ 2% B27 supplement without insulin, 200 μM L-ascorbic
22 acid 2-phosphate sesquimagnesium salt hydrate (Sigma) and 1% Penicillin/Streptomycin
23 (ThermoFisher Scientific), and the small molecules 25 ng/ml Activin A (R&D systems), 30 ng/ml
24 Bone morphogenic protein-4 (BMP4) (R&D systems), 1.5 μM CHIR99021 (Stemgent), and 50
25 ng/ml Vascular Endothelial Growth Factor type A (VEGF-A) (Peprotech) for 3 days (no media
26 changes). Endothelial cell fate was further specified with RPMI B27- medium supplemented with
27 50 ng/ml VEGF-A and 10 μM SB431542 with media changes every 2 to 3 days until day 8.

28 **FACS sorting endothelial cells**

29 Endothelial cells were harvested after 8 d of differentiation using TrypLE (ThermoFisher
30 Scientific). Single cells were separated using a 100 μm strainer and labelled with CD31 antibody
31 (1:200, M082329-2, DAKO) at 4°C for 45 min followed by 30 min staining with a goat anti-
32 mouse secondary antibody conjugated to AlexaFluor 488 or 555 (1:400, A-11001 and A-21422,
33 ThermoFisher Scientific). Cells were analysed using Becton Dickinson FACSAria II, gated on
34 forward and side scatter. Single cells were identified and sorted based on CD31+ expression.
35 CD31+ endothelial cells were expanded in EGM-2 (Lonza) in Matrigel flasks and cryopreserved.

36 **hCO fabrication**

37 hCO culture inserts were fabricated using SU-8 photolithography and PDMS molding (Mills et
38 al., 2017a). Differentiated cells were mixed at ratio of 20% endothelial cells and 80%
39 cardiomyocytes/fibroblasts to form hCO. Acid-solubilized bovine collagen 1 (Devro) was salt
40 balanced using 10x DMEM (ThermoFisher Scientific) and pH neutralized using 0.1M NaOH
41 before combining with Matrigel and then the cell suspension on ice. Each hCO contained 5 x
42 10^4 cells, a final concentration of 2.6 mg/ml collagen I and 9% Matrigel. 3.5 μL of suspension
43 was pipetted into the hCO culture insert and incubated at 37°C with 5% CO_2 for 45 min in order
44 to gel. After gelling, α-MEM GlutaMAX (ThermoFisher Scientific), 10% fetal bovine serum (FBS),
45 200 μM L-ascorbic acid 2-phosphate sesquimagnesium salt hydrate (Sigma) and 1%
46 Penicillin/Streptomycin (ThermoFisher Scientific) was added. hCO were subsequently cultured
47 in maturation media (MM) (Mills et al., 2017a) with medium changes every 2 to 3 days for 5
48 days (7 days old hCO). To better approximate adult metabolic provisions a 'weaning medium'

(WM) was utilized. hCO were cultured in WM containing 4% B27 – insulin, 5.5 mM glucose, 1 nM insulin, 200 µM L-ascorbic acid 2-phosphate sesquimagnesium salt hydrate, 1% P/S, 1% GlutaMAX (100x), 33 µg/mL aprotinin and 10 µM palmitate (conjugated to bovine serum albumin in B27) in DMEM without glucose, glutamine and phenol red (ThermoFisher Scientific) with media changes every 2-3 days.

Force analysis of hCO

The elasticity of the Heart Dyno poles enables the contractile properties to be determined via tracking pole deflection, which directly correlates with force (Mills et al., 2017a). Videos of 10 seconds were made of each hCO with the Nikon ANDOR WD Revolution Spinning Disk microscope (magnification 4x). While imaging, hCO were incubated at 37°C, 5% CO_2 to prevent changes in contractile behaviour. For pacing, hCOs were electrically stimulated at 1 Hz with 5 ms square pulses with 20 mA current using a Panlab/Harvard Apparatus Digital Stimulator. Videos were then analysed with a custom written Matlab program (Mills et al., 2017a). This facilitated the analysis of the contractile properties of the organoids and the production of time-force graphs (Mills et al., 2017a). Moreover, data was obtained regarding additional important functional parameters including the contraction rate and the activation and relaxation time of the organoids.

Immunostaining of hCO (endothelial)

hCO were fixed with 1% paraformaldehyde (Sigma) for 1 h. Cells were stained with primary antibodies CD31 (1:200, M082329-2, DAKO), NG2 (1:200, 14-6504-82, ThermoFisher Scientific) and cardiac troponin T (1:400, ab45932, Abcam) in 5% FBS and 0.25% TritonX-100 Blocking Buffer at 4°C overnight on a rocker. Cells were washed twice for 1 h with Blocking Buffer and labelled with secondary antibodies goat anti-mouse IgG_1 AlexaFluor 488 (1:400, A-21121), goat anti-mouse IgG_{2a} AlexaFluor 555 (1:400, A-21137) and goat anti-rabbit IgG AlexaFluor 633 (1:400, A-21070) and Hoechst33324 (all ThermoFisher Scientific) at 4°C overnight on a rocker. Cells were again washed with Blocking Buffer twice for 1 h and mounted on microscope slides using ProLong Glass (ThermoFisher Scientific).

Phosphoproteomics

Phosphoproteomics experiments were performed with biological triplicates. Phosphopeptides were enriched from 20 pooled hCO, yielding approximately 100 µg of total protein per condition. The high-sensitivity EasyPhos workflow was employed as previously described (Humphrey et al., 2018). Briefly, pooled organoids were lysed in SDC buffer (4% Sodium deoxycholate, 100 mM Tris pH 8.5) and immediately heated for 5 min at 95°C. Lysates were cooled on ice, and sonicated with a tip-probe sonicator (50% output power, 30 seconds). An aliquot of lysate was taken and diluted 1:5 in 8 M Urea from which protein concentration was determined by BCA assay (Thermo Fisher Scientific). Aliquots corresponding to 100 µg of protein were subsequently diluted in SDC buffer into a 96-well deep-well plate, reduced and alkylated at 45°C for 5 min by the addition of 10 mM Tris (2-carboxyethyl)phosphine (TCEP)/40 mM 2-Chloroacetamide (CAA) pH 8, and digested by the addition of 1:100 Lys-C and Trypsin overnight at 37°C with agitation (1,500 rpm). After digestion phosphopeptides were enriched in parallel according to the EasyPhos workflow as described (Humphrey et al., 2018). Eluted phosphopeptides were dried in a SpeedVac concentrator (Eppendorf) and resuspended in MS loading buffer (0.3% TFA/2% acetonitrile) prior to LC-MS/MS measurement.

LC-MS/MS Measurement

Phosphopeptides were loaded onto a 40 cm column fabricated in-house with 75 µM inner diameter fused silica packed with 1.9 µM C18 ReproSil particles (Dr. Maisch GmBH). A column oven (Sonation) was used to maintain column temperature at 60°C, and a U3000 HPLC system

(Dionex, Thermo Fisher Scientific) was connected to a Q Exactive HF X benchtop Orbitrap mass spectrometer (Thermo Fisher Scientific) with a NanoSpray Flex ion source (Thermo Fisher Scientific). For all samples, peptides were separated using a binary buffer system of 0.1% (v/v) formic acid (buffer A) and 80% (v/v) acetonitrile/0.1% (v/v) formic acid (buffer B). Peptides were eluted at a flow rate of 400 nl/min and separated with a gradient of 3 − 19% buffer B over 40 minutes, followed by 19 − 41% buffer B over 20 minutes, and peptides were analysed with a full scan (350 − 1,400 m/z; R=60,000 at 200 m/z) at a target of 3e6 ions, followed by up to ten data-dependent MS2 scans using HCD (target 1e5; max. IT 50 ms; isolation window 1.6 m/z; NCE 27%; min. AGC target 2e4), detected in the Orbitrap mass analyser (R=15,000 at 200 m/z). Dynamic exclusion (30 s) and Apex trigger (2 to 4 s) were enabled.

MS data processing

RAW MS data was processed in the MaxQuant software environment (Cox and Mann, 2008) (version 1.6.0.9), searching against the Human UniProt Reference database (December 2019 release), using default settings with the addition of 'Phospho(STY)' as a variable modification and 'Match between runs' switched on for all analyses. Data analysis was performed using the Perseus software package (Tyanova and Cox, 2018).

Single nuclei RNA-sequencing of hCO

Pooled hCO (~40) were homogenized in 4 mL lysis buffer (300 mM sucrose, 10 mM Tris-HCl (pH = 8), 5 mM CaCl$_2$, 5 mM magnesium acetate, 2 mM EDTA, 0.5 mM EGTA, 1 mM DTT)(all Sigma-Aldrich) with 30 strokes of a dounce tissue grinder (Wheaton). Large pieces of hCO were allowed to settle and homogenate was passed through pre-wetted 40 µm cell strainers (Becton Dickinson). Remaining hCO material in the douncer was resuspended in 4 ml and the douncing and filtering steps were repeated twice. All steps of the homogenization were performed on ice. The filtered homogenate was centrifuged at 1500 x g for 5 min at 4°C. Nuclei pellets were then re-suspended in PBS. A fraction of resuspended nuclei were then stained with Hoechst33324 nuclear stain (1:500 dilution) and counted on a haemocytometer under fluorescent microscope.

The nuclei were then re-centrifuged (1500 x g for 5 min at 4°C) and resuspended at a density to load ~5,000 nuclei per sample. Cells were loaded into the Chromium Controller (10X Genomics) for gel bead emulsion (GEM) formation. Library preparation was conducted according to the manufacturer's recommended protocol using the Chromium Next GEM Single Cell 3' GEM, Library & Gel Bead Kit v3.1. Libraries were sequenced on the NextSeq 500/550 v2 (Illumina) with 150 bp reads and were sequenced to ~250,000 reads per cell.

Raw fastq reads for each sample were processed using CellRanger v3.1.0. Default options were used with CellRanger and a custom made pre mRNA reference using GRCh38 v3.0.0 was used to map the reads and for count quantification with the CellRanger counts tool. Following this, the counts were then aggregated together to create a single matrix that contained all the samples. Reads from the single nuclei sequencing data were aligned to a human pre-mRNA GRCh38 reference genome. All pre-processing and filtering steps of the datasets were subsequently carried out via the Python package Scanpy (https://scanpy.readthedocs.io/en/stable/) (Wolf et al., 2018). Briefly, there was an initial filtering step for genes that are expressed in 3 or more cells and cells with at least 200 detected genes, subsequently removing cells displaying high expression of mitochondrial genes using a cut-off of 4%. We then filtered out cells that had a count depth with a threshold of under 2,000 and higher than 40,000 to remove debris and potential doublets. Gene expression was subsequently normalized for each cell by total expression, scaled by 10,000 and log scaled. Highly variable genes were then identified for clustering. Leiden clustering with an initial resolution of 0.2 was performed to identify clusters within the data. A published human cardiac snRNA-seq dataset

was then used to identify overlap of marker gene sets for main human heart cell types (e.g. cardiomyocytes, fibroblasts, epicardium, pericytes, etc) with the clusters of our dataset, and were labelled accordingly (Tucker et al., 2020). Further refined clustering was carried out on specific clusters that showed overlap of more than one of the various heart cell types. Visualization of the datasets was primarily carried out using nonlinear dimensionality reduction UMAP plots (Becht et al., 2019). In the snRNA-seq we note the lower than expected percentage of non-myocytes and the loss of endothelial cells (Mills et al., 2017a; Voges et al., 2017), indicating the protocol requires further optimization for hCO samples.

hCO comparison to bulk nuclei RNA sequencing data for PCA

Nuclear RNA-seq dataset generated from sorted cardiomyocyte nuclei at two stages (fetal and adult) was obtained from BioProject ID: PRJNA353755 (Gilsbach et al., 2018). RNA-seq dataset was mapped to the human genome (hg38) using STAR aligner (version 2.7.3a). Annotations and genome files (hg38) were obtained from *Ensembl (release 102)*. Uniquely mapped reads were counted across genes with a program in Bioconductor R (Huber et al., 2015) package, featureCounts (version 2.0.1) (Liao et al., 2014). Subsequent analyses of the count data were performed in the R statistical programming language with the Bioconductor packages edgeR (Robinson et al., 2010) and the annotation package org. Hs.eg.db. In this dataset, only genes with > 0.5 counts per million (CPM) in at least 4 samples were retained for statistical analysis. Additionally, ribosomal and mitochondrial genes as well as pseudogenes, and genes with no annotation (Entrez Gene identification) were removed before normalization and statistical analysis.

Principal component analysis (PCA) performed using the intersection of the 25% most highly variable genes of the snRNA-seq dataset and genes expressed in the bulk samples. Each of the two datasets were log transformed and scaled separately before running the dimensionality reduction method.

Pro-inflammatory stimulation of hCO

Cytokines (human) and factors were added individually and in combinations in WM: 100 ng/ml TNF, 10 ng/ml IL-1β, 100 ng/ml IFN-γ, 100 ng/ml IL-6, 100 ng/ml IL-17A, 100 ng/ml G-CSF (Amgen), 10 µg/ml poly(I:C) (HMW, Invivogen) or 1 µg/ml LPS (from *Escherichia coli* strain 0127:B8, Sigma) (all Peprotech unless noted). Additional concentrations were performed for the dose-response curves for TNF, IL-1β, IFN-γ and poly(I:C) as indicated. The function of hCO was determined before addition of these factors as a baseline (time 0 h) and any changes normalized to the original baseline and to the control. The medium was not exchanged unless noted.

Drug screening

Compounds were sources from MedChem Express (unless noted) and dissolved at 10 mM in DMSO and vehicle controls used. A larger batch of INCB054329 was sourced from Selleckchem. The following compounds were used at 2 or 3 doses previously shown to have *in vitro* efficacy as per the reference papers for: JQ-1 (Selleckchem), INCB054329, ABBV-744, ruxolitinib, baricitinib, flavopiridol, SEL120-34A, BI-1347, and paroxetine hydrochloride. Additional compounds tested were molibresib, alobresib, and apabetalone. For some experiments apabetalone and RVX-2157 were sent blinded by Resverogix. Compounds were given at the time of pro-inflammatory factor addition, except for experiments with baricitnib and INCB054329 where recovery of function was also assessed by addition 24 h following addition of inflammatory factors.

Linear regression of cytokine storm responses

To determine factor effects, second order OLS linear regression was performed across all relevant samples using binary predictors (cytokine presence/absence) with force, relaxation/activation times as the outcome variables. p-values were determined using two-tailed t-tests. Normality (Shipiro-Wilks), heteroskedasticity (Breusch-Pagan), linearity (Harvey-Collier), multicollinearity (condition no.) and skewness/kurtosis (Jarque-Bera) were all checked with the respective tests. The coefficient of determination, R^2 (adjusted), was used to determine goodness of fit.

SARS-CoV-2 K18-hACE2 mouse infection model

Female K18-hACE2 mice were lightly anesthetized using isoflurane and 50 µl of SARS-CoV-2 at 5×10^4 TCID50 per mouse was administered via intranasal inoculation (i.n.). On 1, 2 and 3 dpi, INCB054329 or placebo control was administered via oral gavage. Mice were randomized and received either vehicle 30% (m/v) Kolliphor 15 HS (Sigma) in PBS or 2 mg per 30 g mouse body weight of INCB054329 at 20 mg/ml in the Kolliphor solution (66.7 mg/kg). At 4 or 5 d.p.i., mice were euthanized by cervical dislocation and heart and lung tissue was fixed in 10% formalin for histology. At 4 d.p.i. lungs or hearts were homogenized in TRIzol for RNA extraction and stored at -80°C.

Bulk RNA-seq from SARS-CoV-2 K18-hACE2 mouse infection model

Illumina Stranded Total RNA Prep with Ribo-Zero Plus kits were used to prepare total RNA for sequencing. Libraries were sequenced on the NextSeq 500/550 v2 (Illumina) with 150 bp reads and were sequenced to ~60,000,000 reads per sample. Sequence reads were trimmed for adapter sequences using Cutadapt version1.9 (Martin, 2011) and aligned using STAR version 2.5.2a (Dobin et al., 2013) to the Mus Musculus GRCm38 assembly with the gene, transcript, and exon features of Ensembl (release 102) gene model, and the SARS-CoV-2 Ensembl genome assembly ASM985889v3. Quality control metrics were computed using RNA-SeQC version 1.1.8 (DeLuca et al., 2012) and expression was estimated using RSEM version 1.2.30 (Li and Dewey, 2011). Protein-coding genes with > 5 CPM in ≥ 5 samples were kept for further analysis. Trimmed mean of M-values (TMM) normalization and differential expression analysis were performed using the R package edgeR (Robinson et al., 2010). The glmQLFit() function was used to fit a quasi-likelihood negative binomial generalised log-linear model to the read counts for each gene. Using the glmQLFTest() function, we conducted gene-wise empirical Bayes quasi-likelihood F-tests for a given contrast. Differentially expressed genes (DEGs) were determined using absolute log2 fold change (logFC) > 0.5 and a false discovery rate (FDR) < 0.05. The function prcomp() was used for principal component analysis (PCA). To estimate SARS-CoV-2 replication levels, sequence reads were aligned to SARS-CoV-2 only, and samtools (Li et al., 2009) version 1.9 was used to estimate the mapping rate of the reads to the viral genes.

Comparison of different RNA-seq data

KEGG and Encode TF analyses was performed using Enrichr (Kuleshov et al., 2016). BioMart Ensembl (release 102) was used to obtain the mouse to human orthologues used in comparisons. Networks were generated through the use of Ingenuity Pathway Analysis (IPA) on DEGs (QIAGEN Inc., https://www.qiagenbioinformatics.com/products/ingenuity-pathway-analysis). Up-Stream Regulators enriched in differentially expressed genes (no logFC cutoff, FDR < 0.05) in direct and indirect interactions were investigated by performing Core Analysis using (QIAGEN).

Quantitative RT-PCR

RNA was extracted using QIAGEN RNAeasy Micro Kits (Qiagen) or Trizol. cDNA synthesis using Superscript III (ThermoFisher Scientific) was carried out as per manufacturer's

1　instructions. Final primer concentration of 200-250 nM was used and gene expression was
2　assessed over 40 cycles on an Applied Biosciences Quant Studio 5. *18S* (for viral infection
3　studies) or *HPRT1* or *hprt* (for gene expression) were used as internal controls.

4　*Human*

5　RNA18S5　　　　Fwd GCTGAGAAGACGGTCGAACT　　　　Rev CGCAGGTTCACCTACGGAAA

6　HPRT1　　　　　Fwd AACCTCTCGGCTTTCCCG　　　　　Rev TCACTAATCACGACGCCAGG

7　LGALS3BP　　　Fwd TGTGGTCTGCACCAATGAAAC　　　Rev CTGCACATTCACGCTGATGG

8　BRD4　　　　　Fwd CTGACAGCGAAGACTCCGA　　　　Rev GTGGTGATGATGGTGCTTCTTC

9　*Mouse*

10　Hprt　　　　　Fwd AGGCCAGACTTTGTTGGATTTGAA　Rev CAACTTGCGCTCATCTTAGGCTTT

11　Lgals3bp　　　Fwd TCTCTTGCTCCCAGGGTTG　　　　Rev CCTGGAACCAGCAAGAACAC

12　*SARS-CoV-2*

13　E-Gene　　　　Fwd ACAGGTACGTTAATAGTTAATAGCGT　Rev ATATTGCAGCAGTACGCACACA

Mouse LPS cytokine storm model

15　LPS (from *Escherichia coli* strain 0127:B8, Sigma) suspended in PBS was injected
16　intraperitoneally into mice at 0.6 mg per 30 g mouse body weight for inflammatory cytokine,
17　gene expression and survival studies and 1 mg was used for cardiac function studies. After the
18　injection of LPS mice were randomized and received either vehicle 30% (m/v) Kolliphor 15 HS
19　(Sigma) in PBS or 2 mg per 30 g mouse body weight of INCB054329 at 20 mg/ml in the
20　Kolliphor solution (66.7 mg/kg). Treatment groups were blinded. For the experiments, mice were
21　closely monitored and checked hourly for signs of sepsis.

Mouse LPS plasma cytokine assays

23　Serum cytokine levels (Ifn-γ, Il-1β and Tnf) were determined with a CBA Flex Set Multiplex
24　Cytokine Bead Array (BD Biosciences).

Cardiac function *in vivo*

26　Cardiac function was assessed using a Vevo 2100 ultrasound system fitted with a MS550D
27　transducer, which has a 40 MHz center frequency (Fujifilm Visualsonics). Depilated mice were
28　anaesthetized by isoflurane inhalation (1.5% at 1 L oxygen / min) delivered via a nose cone,
29　kept warm on a heated stage, with respiration and heart rate monitored on ECG pads. B Mode
30　images of the left ventricle were obtained from three short-axis views (proximal, mid and distal
31　positions) and one parasternal long-axis view. Cardiac function parameters were calculated
32　using the Simpson's tool in Vevolab analysis software v3.2.6 (Fujifilm Visualsonics). Briefly, the
33　endocardial areas were traced from all three short-axis views, and the length of the ventricle
34　was determined, in systole and diastole. These measurements were used to calculate ejection
35　fraction.

ELISA

37　Human CNTI ELISA (RayBiotech), IFN-γ (RnD Systems) and BNP ELISA (Abcam) was used as
38　per manufacturer's instructions.

Immunoblotting

40　Protein from 2D hPSC-cardiac cell cultures was extracted using RIPA lysis buffer supplemented
41　with protease inhibitor cocktail (Roche). Protein lysate concentration was estimated using a
42　BCA assay (ThermoFisher Scientific). 15 μg protein was resolved on 4-12% Bis-Tris
43　polyacrylamide gel (Invitrogen) at 200V for 20 min and then transferred at 20 V for 1 h onto
44　polyvinylidene difluoride (PVDF) membrane as per manufacturer's recommendations. After 1 h

1   blocking using a 1:1 mix of LI-COR Odyssey Blocking Buffer (LI-COR Biotechnology) and PBS,
2   membranes were incubated overnight on a platform shaker with primary antibodies for ACE2
3   (1:200, R&D Systems, AF933) and GAPDH (1:1000, Cell Signaling Technologies, 97166S).
4   Membranes were washed 5 times 3 minutes in PBS with 0.5% Tween, prior to incubation with
5   IRDye® secondary antibodies (1:10000 for IRDye® 800CW Goat anti-Mouse IgG Secondary
6   Antibody, 926-32210, and 680RD Donkey anti-Goat IgG Secondary Antibody, LI-COR
7   Biotechnology, 925-68074) for 1 h at room temperature. Membranes were washed thoroughly (5
8   x 3 min in PBS + 0.5% Tween) and were then imaged on a LI-COR Odyssey® CLx.
9   Densitometry was performed using ImageStudio Lite (version 4).

10 **Flow Cytometry for ACE2 and SARS-CoV-2 spike binding assays**

11 hPSC-cardiac cells were differentiated as above, then plated at 100,000 per cm^2 on gelatin
12 coated plates and cultured for 5 days prior to infection experiments. For 2D cultured hPSC-CM,
13 cells were pre-treated with MM with or without the indicated compounds or DMSO as a vehicle
14 control for 3 days prior to assays. Cells were was 2 x with PBS and detached using 0.25%
15 Trypsin/EDTA (ThermoFisher Scientific) for ~10-15 min at 37°C. This was then neutralized with
16 equivolume 3% bovine serum albumin (Sigma) in PBS (Binding Buffer). Cells were then
17 centriguged at 300 x g for 3 min and the supernatant removed. Cells were then incubated under
18 different conditions.

19 For ACE2 assays the following was used for control, 1:200 Goat IgG Alexa Fluor 647-
20 conjugated antibody, and assay 1:200 anti-human ACE2 AlexFluor 647 conjugated antibody
21 and 1:200 anti-human CD90 (all RnD Systems) and were incubated for 60 min at 4°C in Binding
22 Buffer. The cells were then washed in Binding Buffer, centrifuged at 300 x g for 3 min and
23 supernatant removed. Both conditions were then incubated with 1:400 goat anti-mouse IgG
24 secondary antibody conjugated to Alexa Fluor 555 (ThermoFisher Scientific) in Binding Buffer
25 for 45 min at 4°C. The cells were then washed in Binding Buffer, centrifuged at 300 x g for 3 min
26 and supernatant removed.

27 For SARS-CoV-2 binding assays the following was used for control, Binding Buffer only, and
28 assay 1 µg rSARS-CoV-2 Spike RB (per ~100,000 cells) and 1:200 anti-human CD90 (all RnD
29 Systems) and were incubated for 60 min at 4°C in binding buffer. The cells were then washed in
30 Binding Buffer, centrifuged at 300 x g for 3 min and supernatant removed. Both conditions were
31 then incubated with 1:400 F(ab')2-goat anti-human IgG Fc secondary antibody conjugated to
32 Alexa Fluor 488 and 1:400 goat anti-mouse IgG secondary antibody conjugated to Alexa Fluor
33 555 (both ThermoFisher Scientific) in Binding Buffer for 45 min at 4°C. The cells were then
34 washed in binding buffer, centrifuged at 300 x g for 3 min and supernatant removed.

35 For flow cytometry cells were resuspended in 300 µl Binding Buffer, put through a 100 µm cell
36 strainer to remove any clumps. Cells were assessed on a BD LSRFortessa Flow Cytometer,
37 gated on FSC-A/SSC-A and then remove doublets using FSC-W/H, and CD90 assessed using
38 YG586/15, ACE2 using R670/14 and SARS-CoV-2 spike protein B530/30. Negative controls
39 were used to draw gates.

40 **hPSC-CM SARS-CoV-2 infection at QIMR Berghofer**

41 <u>hPSC-cardiac cell infection</u>

42 hPSC-cardiac cells were differentiated as above, then plated at 100,000 per cm^2 on gelatin
43 coated plates and cultured for 5 days prior to infection experiments. For 2D cultured hPSC-CM,
44 cells were pre-treated with 1 ml of MM with or without the indicated compounds or DMSO as a
45 vehicle control for 3 days prior to infection. Media was removed before infecting cells with
46 SARS-CoV-2 at MOI 0.01 for 1 h at 37°C. Cells were washed 3 x with MM and replaced with 1
47 ml of MM with compounds or DMSO. For intracellular RNA cells were washed 3x with PBS

1 before harvesting RNA in Trizol. For supernatant experiments 500 µl of supernatants were
2 harvested each day and replaced with 500 µl of media. Supernatants were frozen at -80°C until
3 they were titred. Titration was performed in Vero cell monolayers in 96 well plates: inoculated
4 serial 10-fold dilutions in quadruplicate and incubated for 4 days. Cytopathic effect recorded and
5 virus titre in log10 $TCID_{50}$/ml recorded.

6 Imaging

7 For immunostaining cells or hCO were fixed in 4% paraformaldehyde and stained. Cells were
8 stained with primary antibodies Nucleocaspid protein SARS-CoV-2 (1:200, 40143-MM05, Sino
9 Biological) and cardiac troponin T (1:400, ab45932, Abcam) in Blocking Buffer at 4°C for 2 h for
10 2D or overnight for hCO on a rocker. Cells were washed twice with Blocking Buffer and labelled
11 with secondary antibodies goat anti-mouse IgG AlexaFluor 488 (1:400, A-11001) and goat anti-
12 rabbit IgG AlexaFluor 555 (1:400, A-21428) and Hoechst3332 (all ThermoFisher Scientific) at
13 4°C for 2 h for 2D or overnight for hCO on a rocker. Cells were again washed with Blocking
14 Buffer twice and then put into PBS and were imaged using a Leica Thunder microscope.

15 Quantitative RT-PCR

16 Performed as described above.

17 **hPSC-CM SARS-CoV-2 infection experiments at The Peter Doherty Institute**

18 hPSC-CM infection

19 The female human embryonic stem cell line HES3 NKX2-5$^{eGFP/w}$ was used for viral infection
20 studies in 2D monolayer cultures (Elliott et al., 2011). Cardiac cells were differentiated as
21 previously described (Anderson et al., 2018), frozen at day 10 following differentiation and
22 stored at -80°C. Cardiac cells were subsequently thawed in RPMI+B27 media (RPMI 1640
23 supplemented with 2% B-27 Supplement minus vitamin A, 1% GlutaMAX and 1%
24 Penicillin/Streptomycin- All from ThermoFisher Scientific) with Rock inhibitor (Selleck
25 Chemicals) for 24 h. Cardiac cells were then maintained in RPMI + B27 media for an additional
26 2 days, enriched for cardiomyocytes with lactate purification media - DMEM, no glucose, no
27 glutamine, no phenol red supplemented with 1% GlutaMAX and 1% Penicillin/Streptomycin
28 (Thermo Fisher Scientific) and 5 mM Sodium L-Lactate (Sigma Aldrich) for 2 days, and
29 subsequently cultured in MM from day 15 to day 23 post differentiation prior to viral infection.

30 The media was removed from cultures of cardiac myocytes and Vero cells in 24 well plates.
31 Vero cell plates were washed with 1ml of serum free media per well. Media was removed, wells
32 were inoculated with 10^4 $TCID_{50}$ of virus (MOI = 0.01) in 100 µl serum free media and incubated
33 for 1 h at room temperature. The inoculum for Vero cells incorporated TPCK-treated Trypsin
34 (Worthington Biochemical Corporation) at 1 µg/ml. Following virus adsorption, the inoculum was
35 removed and replaced with 500 µl media. After ~10 minutes, this was removed and stored at -
36 80°C as the day 0 sample. 500 µl per well of media was replenished and plates were incubated
37 at 37°C in 5% CO2. Each day from day 1 through 6 post-infection, 500 µl of culture supernatant
38 was harvested and replenished with 500 µl of media. Supernatants were stored at -80°C till they
39 were titrated.

40 Virus titration

41 The amount of infectious virus present in the samples was assayed in Vero cell monolayers in
42 96 well plates. Samples inoculated into 4 wells were diluted serially in 10-fold dilutions in serum
43 free media containing 1 µg/ml TCPK-treated Trypsin and incubated for at 37°C in 5% CO2.
44 Cytopathic effect was scored on day 4 post-infection and virus titre expressed in log_{10}
45 $TCID_{50}$/ml. The lower limit of detection was 1.7 log_{10} $TCID_{50}$/ml.

1 **SOMAscan™ Proteomic Analysis**

2 SOMAScan[TM] proteomic technology uses Somamers as an affinity reagent (Somalogic Inc.).
3 Plasma samples from 47 patients from each group that received apabetalone or placebo in the
4 ASSURE trial were analysed and LGALS3BP quantified (Nicholls et al., 2016).

5 **QUANTIFICATION AND STATISTICAL ANALYSIS**

6 Statistics were performed using GraphPad Prism v8 unless noted with the appropriate tests
7 outlined in the Figure legends.

8 hCO force experiments were performed on quality controlled hCO (proper formation around the
9 poles, non-arrhythmic, no broken arms, no necking (Mills et al., 2017a) across multiple
10 experiments with multiple cell line combinations to ensure reproducibility. Automated force
11 analysis removes the requirement for blinding of hCO experiments. Personnel performing the
12 animal experiments and analyses were blinded to the conditions or treatments.

13

1 **KEY RESOURCES TABLE**

REAGENT or RESOURCE	SUPPLIER	IDENTIFIER
Antibodies		
Mouse anti-human CD31	Dako	RRID: AB_2114471
Neural/Glial Antigen 2	Life Technologies	RRID: AB_10870987
Rabbit anti-cardiac Troponin T	Abcam	RRID: AB_956386
Mouse IgG2a anti-Human CD90	RnD Systems	RRID: AB_2203306
Human ACE-2 Alexa Fluor 647-conjugated antibody	RnD Systems	CAT# FAB933R
Goat IgG Alexa Fluor 647-conjugated Antibody	RnD Systems	CAT# IC108R
Goat anti-human ACE2 polyclonal antibody	RnD Systems	RRID: AB_355722
SARS-CoV-2 Nucleocapsid Antibody, Mouse MAb	Sino Biological	RRID: AB_2827977
Mouse Anti-GAPDH Monoclonal Antibody	Cell Signaling Technology	RRID:AB_2756824
Goat anti-Mouse IgG1 Cross-Adsorbed Secondary Antibody, Alexa Fluor 488	ThermoFisher Scientific	RRID: AB_2535764
Goat anti-Mouse IgG2a Cross-Adsorbed Secondary Antibody, Alexa Fluor 555	ThermoFisher Scientific	RRID: AB_2535776
Goat anti-Mouse IgG (H+L) Cross-Adsorbed Secondary Antibody, Alexa Fluor 488	ThermoFisher Scientific	RRID: AB_2534069
Goat anti-Mouse IgG (H+L) Cross-Adsorbed Alexa Fluor 555	ThermoFisher Scientific	RRID: AB_2535844
F(ab')2-Goat anti-Human IgG Fc Secondary Antibody	ThermoFisher Scientific	RRID: AB_2536548
Goat anti-Rabbit IgG (H+L) Cross-Adsorbed Secondary Antibody, Alexa Fluor 555	ThermoFisher Scientific	RRID: AB_2535849
Goat anti-Rabbit IgG (H+L) Cross-Adsorbed Secondary Antibody, Alexa Fluor 633 use 1:400	ThermoFisher Scientific	RRID:AB_2535731
IRDye®800CW Goat anti-Mouse IgG Secondary Antibody	LI-COR Biotechnology	RRID AB_621842
IRDye®680RD Donkey anti-Goat IgG Secondary Antibody	LI-COR Biotechnology	RRID AB_2650427
Proteins		
rSARS-CoV-2 Spike RB	RnD Systems	CAT# 10499CV100
ELISA		
Human CNTI ELISA	RayBiotech	CAT# ELH-CTNI-1
BNP ELISA	Abcam	CAT# ab193694
IFN-γ ELISA	RnD Systems	CAT# DIF50C
Mouse Inflammation Kit Cytokine Bead Array	BD Biosciences	CAT# 552364
Deposited Data		
Phospho-Proteomics data of vascularised cardiac organoids	This study	PRIDE: PXD020994
RNA-seq of mouse heart maturation	(Gilsbach et al., 2018)	BioProject ID: PRJNA353755
Bulk RNA-seq of SARS-CoV2 infected K-18 mice	This study	ENA EGAS00001004626
snRNA-seq of vascularised cardiac organoids	This study	ENA: EGAS00001004626
Experimental Models: Cell Lines		
Human embryonic stem cell line HES3	WiCell	RRID: CVCL_7158
Human induced pluripotent stem cell line RM3.5	Murdoch Children's Research Institute	N/A
Human induced pluripotent stem cell line AA	CIRM hPSC Repository	CW30382A

Human induced pluripotent stem cell line CC	CIRM hPSC Repository	CW30318C
Experimental Models: Organisms/Strains		
C57BL/6J mice		RRID: MGI: 3028467
K18-hACE2 C57BL/6J mice (strain B6.Cg-Tg(K18-ACE2)2Prlmn/J)		RRID:IMSR_JAX:034860
SARS-CoV2 (QIMR Berghofer)		hCoV-19/Australia/QLD02/2020
SARS-CoV2 (The Doherty Institute)		CoV/Australia/VIC01/2020
Oligonucleotides		
Primers for qPCR, see Table KR1		
Software and Algorithms		
Pole tracking analysis	(Mills et al., 2017b)	N/A
MaxQuant	(Cox and Mann, 2008)	RRID:SCR_014485
Perseus	(Tyanova and Cox, 2018)	RRID:SCR_015753
STAR aligner	(Dobin et al., 2013)	RRID:SCR_015899
CellRanger		RRID:SCR_017344
Cutadapt	(Martin, 2011)	RRID:SCR_011841
RNA-SeQC	(DeLuca et al., 2012)	RRID:SCR_005120
RSEM	(Li and Dewey, 2011)	RRID:SCR_013027
Scanpy	(Wolf et al., 2018)	RRID:SCR_018139
Bioconductor R	(Huber et al., 2015)	RRID: SCR_001905
Bioconductor packages edgeR	(Robinson et al., 2010)	RRID:SCR_012802

1

1 **VIDEO LEGENDS**

2 **Supplementary Video 1:** Human cardiac organoids cultured under CTRL conditions. The video
3 was taken over a period of 10 seconds and is displayed in real time (50 frames/s). Related to
4 Figure 1.

5 **Supplementary Video 2:** Human cardiac organoids after treatment with cardiac cytokine storm.
6 The video was taken over a period of 10 seconds and is displayed in real time (50 frames/s).
7 Related to Figure 1.

8 **Supplementary Video 3:** Human cardiac organoids cultured under CTRL conditions and paced
9 at 1 Hz. The video was taken over a period of 5 seconds and is displayed in real time (50
10 frames/s). Related to Figure 1.

11 **Supplementary Video 4:** Human cardiac organoids after treatment with cardiac cytokine storm
12 and paced at 1 Hz. The video was taken over a period of 5 seconds and is displayed in real time
13 (50 frames/s). Related to Figure 1.

14 **Supplementary Video 5:** Human cardiac organoids cultured after treatment with cardiac
15 cytokine storm and 1µM INCB054329. The video was taken over a period of 10 seconds and is
16 displayed in real time (50 frames/s). Related to Figure 4.

17

1 **EXCEL TABLE TITLES**

2 **Supplemental Table 1:** Bioinformatic analyses on RNA-sequencing data. Related to Figure 5..
3 Related to Figure 5.

4 **Supplemental Table 2:** Patient data for COVID-19 plasma and serum samples. Related to
5 Figure 6.

REFERENCES

Anand, P., Brown, J.D., Lin, C.Y., Qi, J., Zhang, R., Artero, P.C., Alaiti, M.A., Bullard, J., Alazem, K., Margulies, K.B.*, et al.* (2013). BET bromodomains mediate transcriptional pause release in heart failure. Cell *154*, 569-582.10.1016/j.cell.2013.07.013

Anderson, D.J., Kaplan, D.I., Bell, K.M., Koutsis, K., Haynes, J.M., Mills, R.J., Phelan, D.G., Qian, E.L., Leitoguinho, A.R., Arasaratnam, D.*, et al.* (2018). NKX2-5 regulates human cardiomyogenesis via a HEY2 dependent transcriptional network. Nature communications *9*, 1373.10.1038/s41467-018-03714-x

Antolic, A., Wakimoto, H., Jiao, Z., Gorham, J.M., DePalma, S.R., Lemieux, M.E., Conner, D.A., Lee, D.Y., Qi, J., Seidman, J.G.*, et al.* (2020). BET bromodomain proteins regulate transcriptional reprogramming in genetic dilated cardiomyopathy. JCI Insight *5*.10.1172/jci.insight.138687

Arunachalam, P.S., Wimmers, F., Mok, C.K.P., Perera, R.A.P.M., Scott, M., Hagan, T., Sigal, N., Feng, Y., Bristow, L., Tak-Yin Tsang, O.*, et al.* (2020). Systems biological assessment of immunity to mild versus severe COVID-19 infection in humans. Science *369*, 1210-1220.10.1126/science.abc6261

Auguste, G., Rouhi, L., Matkovich, S.J., Coarfa, C., Robertson, M.J., Czernuszewicz, G., Gurha, P., and Marian, A.J. (2020). BET bromodomain inhibition attenuates cardiac phenotype in myocyte-specific lamin A/C-deficient mice. The Journal of clinical investigation *130*, 4740-4758.10.1172/jci135922

Bancerek, J., Poss, Z.C., Steinparzer, I., Sedlyarov, V., Pfaffenwimmer, T., Mikulic, I., Dölken, L., Strobl, B., Müller, M., Taatjes, D.J.*, et al.* (2013). CDK8 kinase phosphorylates transcription factor STAT1 to selectively regulate the interferon response. Immunity *38*, 250-262.10.1016/j.immuni.2012.10.017

Becht, E., McInnes, L., Healy, J., Dutertre, C.-A., Kwok, I.W.H., Ng, L.G., Ginhoux, F., and Newell, E.W. (2019). Dimensionality reduction for visualizing single-cell data using UMAP. Nature biotechnology *37*, 38-44.10.1038/nbt.4314

Chen, C., Li, H., Hang, W., and Wang, D.W. (2020). Cardiac injuries in coronavirus disease 2019 (COVID-19). Journal of Molecular and Cellular Cardiology *145*, 25-29.10.1016/j.yjmcc.2020.06.002

Cochran, A.G., Conery, A.R., and Sims, R.J. (2019). Bromodomains: a new target class for drug development. Nature Reviews Drug Discovery *18*, 609-628.10.1038/s41573-019-0030-7

Cox, J., and Mann, M. (2008). MaxQuant enables high peptide identification rates, individualized p.p.b.-range mass accuracies and proteome-wide protein quantification. Nature biotechnology *26*, 1367-1372.10.1038/nbt.1511

Del Valle, D.M., Kim-Schulze, S., Huang, H.-H., Beckmann, N.D., Nirenberg, S., Wang, B., Lavin, Y., Swartz, T.H., Madduri, D., Stock, A.*, et al.* (2020). An inflammatory cytokine signature predicts COVID-19 severity and survival. Nature Medicine.10.1038/s41591-020-1051-9

DeLuca, D.S., Levin, J.Z., Sivachenko, A., Fennell, T., Nazaire, M.D., Williams, C., Reich, M., Winckler, W., and Getz, G. (2012). RNA-SeQC: RNA-seq metrics for quality control and process optimization. Bioinformatics (Oxford, England) *28*, 1530-1532.10.1093/bioinformatics/bts196

Deutsch, E.W., Csordas, A., Sun, Z., Jarnuczak, A., Perez-Riverol, Y., Ternent, T., Campbell, D.S., Bernal-Llinares, M., Okuda, S., Kawano, S.*, et al.* (2017). The ProteomeXchange consortium in 2017: supporting the cultural change in proteomics public data deposition. Nucleic Acids Res *45*, D1100-d1106.10.1093/nar/gkw936

Dobin, A., Davis, C.A., Schlesinger, F., Drenkow, J., Zaleski, C., Jha, S., Batut, P., Chaisson, M., and Gingeras, T.R. (2013). STAR: ultrafast universal RNA-seq aligner. Bioinformatics (Oxford, England) *29*, 15-21.10.1093/bioinformatics/bts635

Duan, Q., McMahon, S., Anand, P., Shah, H., Thomas, S., Salunga, H.T., Huang, Y., Zhang, R., Sahadevan, A., Lemieux, M.E.*, et al.* (2017). BET bromodomain inhibition suppresses innate inflammatory and profibrotic transcriptional networks in heart failure. Science translational medicine *9*, eaah5084.10.1126/scitranslmed.aah5084

1   Elliott, D.A., Braam, S.R., Koutsis, K., Ng, E.S., Jenny, R., Lagerqvist, E.L., Biben, C., Hatzistavrou, T., Hirst,
2   C.E., Yu, Q.C., *et al.* (2011). NKX2-5(eGFP/w) hESCs for isolation of human cardiac progenitors and
3   cardiomyocytes. Nature methods *8*, 1037-1040.10.1038/nmeth.1740
4   Evron, T., Daigle, T.L., and Caron, M.G. (2012). GRK2: multiple roles beyond G protein-coupled receptor
5   desensitization. Trends Pharmacol Sci *33*, 154-164.10.1016/j.tips.2011.12.003
6   Faivre, E.J., McDaniel, K.F., Albert, D.H., Mantena, S.R., Plotnik, J.P., Wilcox, D., Zhang, L., Bui, M.H.,
7   Sheppard, G.S., Wang, L., *et al.* (2020). Selective inhibition of the BD2 bromodomain of BET proteins in
8   prostate cancer. Nature *578*, 306-310.10.1038/s41586-020-1930-8
9   Feldman, A.M., Combes, A., Wagner, D., Kadakomi, T., Kubota, T., Li, Y.Y., and McTiernan, C. (2000). The
10 role of tumor necrosis factor in the pathophysiology of heart failure. Journal of the American College of
11 Cardiology *35*, 537-544.10.1016/s0735-1097(99)00600-2
12 Filippakopoulos, P., Qi, J., Picaud, S., Shen, Y., Smith, W.B., Fedorov, O., Morse, E.M., Keates, T.,
13 Hickman, T.T., Felletar, I., *et al.* (2010). Selective inhibition of BET bromodomains. Nature *468*, 1067-
14 1073.10.1038/nature09504
15 Gagliano-Jucá, T., Travison, T.G., Kantoff, P.W., Nguyen, P.L., Taplin, M.-E., Kibel, A.S., Huang, G., Bearup,
16 R., Schram, H., Manley, R., *et al.* (2018). Androgen Deprivation Therapy Is Associated With Prolongation
17 of QTc Interval in Men With Prostate Cancer. J Endocr Soc *2*, 485-496.10.1210/js.2018-00039
18 Gilan, O., Rioja, I., Knezevic, K., Bell, M.J., Yeung, M.M., Harker, N.R., Lam, E.Y.N., Chung, C.-w.,
19 Bamborough, P., Petretich, M., *et al.* (2020). Selective targeting of BD1 and BD2 of the BET proteins in
20 cancer and immuno-inflammation. Science, eaaz8455.10.1126/science.aaz8455
21 Gilsbach, R., Schwaderer, M., Preissl, S., Grüning, B.A., Kranzhöfer, D., Schneider, P., Nührenberg, T.G.,
22 Mulero-Navarro, S., Weichenhan, D., Braun, C., *et al.* (2018). Distinct epigenetic programs regulate
23 cardiac myocyte development and disease in the human heart in vivo. Nature communications *9*,
24 391.10.1038/s41467-017-02762-z
25 Goyal, P., Choi, J.J., Pinheiro, L.C., Schenck, E.J., Chen, R., Jabri, A., Satlin, M.J., Campion, T.R., Nahid, M.,
26 Ringel, J.B., *et al.* (2020). Clinical Characteristics of Covid-19 in New York City. New England Journal of
27 Medicine *382*, 2372-2374.10.1056/NEJMc2010419
28 Guo, S., Carter, R.L., Grisanti, L.A., Koch, W.J., and Tilley, D.G. (2017). Impact of paroxetine on proximal
29 β-adrenergic receptor signaling. Cell Signal *38*, 127-133.10.1016/j.cellsig.2017.07.006
30 Guo, T., Fan, Y., Chen, M., Wu, X., Zhang, L., He, T., Wang, H., Wan, J., Wang, X., and Lu, Z. (2020).
31 Cardiovascular Implications of Fatal Outcomes of Patients With Coronavirus Disease 2019 (COVID-19).
32 JAMA Cardiology *5*, 811-818.10.1001/jamacardio.2020.1017
33 Gupta, A., Madhavan, M.V., Sehgal, K., Nair, N., Mahajan, S., Sehrawat, T.S., Bikdeli, B., Ahluwalia, N.,
34 Ausiello, J.C., Wan, E.Y., *et al.* (2020). Extrapulmonary manifestations of COVID-19. Nature Medicine *26*,
35 1017-1032.10.1038/s41591-020-0968-3
36 Hofmann, M.H., Mani, R., Engelhardt, H., Impagnatiello, M.A., Carotta, S., Kerenyi, M., Lorenzo-Herrero,
37 S., Böttcher, J., Scharn, D., Arnhof, H., *et al.* (2020). Selective and Potent CDK8/19 Inhibitors Enhance NK-
38 Cell Activity and Promote Tumor Surveillance. Molecular Cancer Therapeutics *19*, 1018-
39 1030.10.1158/1535-7163.mct-19-0789
40 Horby, P., Lim, W.S., Emberson, J., Mafham, M., Bell, J., Linsell, L., Staplin, N., Brightling, C., Ustianowski,
41 A., Elmahi, E., *et al.* (2020). Effect of Dexamethasone in Hospitalized Patients with COVID-19: Preliminary
42 Report. medRxiv, 2020.2006.2022.20137273.10.1101/2020.06.22.20137273
43 Huang, C., Wang, Y., Li, X., Ren, L., Zhao, J., Hu, Y., Zhang, L., Fan, G., Xu, J., Gu, X., *et al.* (2020). Clinical
44 features of patients infected with 2019 novel coronavirus in Wuhan, China. The Lancet *395*, 497-
45 506.https://doi.org/10.1016/S0140-6736(20)30183-5
46 Huber, W., Carey, V.J., Gentleman, R., Anders, S., Carlson, M., Carvalho, B.S., Bravo, H.C., Davis, S., Gatto,
47 L., Girke, T., *et al.* (2015). Orchestrating high-throughput genomic analysis with Bioconductor. Nature
48 methods *12*, 115-121.10.1038/nmeth.3252

1   Hudson, J., Titmarsh, D., Hidalgo, A., Wolvetang, E., and Cooper-White, J. (2012). Primitive cardiac cells
2   from human embryonic stem cells. Stem cells and development *21*, 1513-1523.10.1089/scd.2011.0254
3   Humphrey, S.J., Azimifar, S.B., and Mann, M. (2015). High-throughput phosphoproteomics reveals in
4   vivo insulin signaling dynamics. Nature biotechnology *33*, 990-995.10.1038/nbt.3327
5   Humphrey, S.J., Karayel, O., James, D.E., and Mann, M. (2018). High-throughput and high-sensitivity
6   phosphoproteomics with the EasyPhos platform. Nature Protocols *13*, 1897-1916.10.1038/s41596-018-
7   0014-9
8   Johnson, B.J., Le, T.T., Dobbin, C.A., Banovic, T., Howard, C.B., Flores Fde, M., Vanags, D., Naylor, D.J.,
9   Hill, G.R., and Suhrbier, A. (2005). Heat shock protein 10 inhibits lipopolysaccharide-induced
10   inflammatory mediator production. The Journal of biological chemistry *280*, 4037-
11   4047.10.1074/jbc.M411569200
12   Kim, S.Y., Zhang, X., Schiattarella, G.G., Altamirano, F., Ramos, T.A.R., French, K.M., Jiang, N., Szweda,
13   P.A., Evers, B.M., May, H.I.*, et al.* (2020). Epigenetic Reader BRD4 (Bromodomain-Containing Protein 4)
14   Governs Nucleus-Encoded Mitochondrial Transcriptome to Regulate Cardiac Function. Circulation *142*,
15   2356-2370.10.1161/circulationaha.120.047239
16   Kotecha, T., Knight, D.S., Razvi, Y., Kumar, K., Vimalesvaran, K., Thornton, G., Patel, R., Chacko, L., Brown,
17   J.T., Coyle, C.*, et al.* (2021). Patterns of myocardial injury in recovered troponin-positive COVID-19
18   patients assessed by cardiovascular magnetic resonance. European heart
19   journal.10.1093/eurheartj/ehab075
20   Kubota, T., McTiernan, C.F., Frye, C.S., Slawson, S.E., Lemster, B.H., Koretsky, A.P., Demetris, A.J., and
21   Feldman, A.M. (1997). Dilated Cardiomyopathy in Transgenic Mice With Cardiac-Specific Overexpression
22   of Tumor Necrosis Factor-α. Circulation research *81*, 627-635.doi:10.1161/01.RES.81.4.627
23   Kuleshov, M.V., Jones, M.R., Rouillard, A.D., Fernandez, N.F., Duan, Q., Wang, Z., Koplev, S., Jenkins, S.L.,
24   Jagodnik, K.M., Lachmann, A.*, et al.* (2016). Enrichr: a comprehensive gene set enrichment analysis web
25   server 2016 update. Nucleic acids research *44*, W90-W97.10.1093/nar/gkw377
26   La Linn, M., Bellett, A.J., Parsons, P.G., and Suhrbier, A. (1995). Complete removal of mycoplasma from
27   viral preparations using solvent extraction. J Virol Methods *52*, 51-54.10.1016/0166-0934(94)00136-5
28   Levick, S.P., and Goldspink, P.H. (2014). Could interferon-gamma be a therapeutic target for treating
29   heart failure? Heart failure reviews *19*, 227-236.10.1007/s10741-013-9393-8
30   Li, B., and Dewey, C.N. (2011). RSEM: accurate transcript quantification from RNA-Seq data with or
31   without a reference genome. BMC Bioinformatics *12*, 323.10.1186/1471-2105-12-323
32   Li, H., Handsaker, B., Wysoker, A., Fennell, T., Ruan, J., Homer, N., Marth, G., Abecasis, G., and Durbin, R.
33   (2009). The Sequence Alignment/Map format and SAMtools. Bioinformatics (Oxford, England) *25*, 2078-
34   2079.10.1093/bioinformatics/btp352
35   Liao, Y., Smyth, G.K., and Shi, W. (2014). featureCounts: an efficient general purpose program for
36   assigning sequence reads to genomic features. Bioinformatics (Oxford, England) *30*, 923-
37   930.10.1093/bioinformatics/btt656
38   Mangalmurti, N., and Hunter, C.A. (2020). Cytokine Storms: Understanding COVID-19. Immunity *53*, 19-
39   25.https://doi.org/10.1016/j.immuni.2020.06.017
40   Martin, M. (2011). Cutadapt removes adapter sequences from high-throughput sequencing reads. 2011
41   *17*, 3.10.14806/ej.17.1.200
42   Messner, C.B., Demichev, V., Wendisch, D., Michalick, L., White, M., Freiwald, A., Textoris-Taube, K.,
43   Vernardis, S.I., Egger, A.S., Kreidl, M.*, et al.* (2020). Ultra-High-Throughput Clinical Proteomics Reveals
44   Classifiers of COVID-19 Infection. Cell systems *11*, 11-24.e14.10.1016/j.cels.2020.05.012
45   Mills, R.J., Parker, B.L., Quaife-Ryan, G.A., Voges, H.K., Needham, E.J., Bornot, A., Ding, M., Andersson,
46   H., Polla, M., Elliott, D.A.*, et al.* (2019). Drug Screening in Human PSC-Cardiac Organoids Identifies Pro-
47   proliferative Compounds Acting via the Mevalonate Pathway. Cell stem cell *24*, 895-
48   907.e896.10.1016/j.stem.2019.03.009

Mills, R.J., Titmarsh, D.M., Koenig, X., Parker, B.L., Ryall, J.G., Quaife-Ryan, G.A., Voges, H.K., Hodson, M.P., Ferguson, C., Drowley, L.*, et al.* (2017a). Functional screening in human cardiac organoids reveals a metabolic mechanism for cardiomyocyte cell cycle arrest. Proceedings of the National Academy of Sciences *114*, E8372-E8381.10.1073/pnas.1707316114

Mills, R.J., Titmarsh, D.M., Koenig, X., Parker, B.L., Ryall, J.G., Quaife-Ryan, G.A., Voges, H.K., Hodson, M.P., Ferguson, C., Drowley, L.*, et al.* (2017b). Functional screening in human cardiac organoids reveals a metabolic mechanism for cardiomyocyte cell cycle arrest. Proceedings of the National Academy of Sciences of the United States of America *114*, E8372-e8381.10.1073/pnas.1707316114

Needham, E.J., Parker, B.L., Burykin, T., James, D.E., and Humphrey, S.J. (2019). Illuminating the dark phosphoproteome. Science Signaling *12*, eaau8645.10.1126/scisignal.aau8645

Nicholls, S.J., Puri, R., Wolski, K., Ballantyne, C.M., Barter, P.J., Brewer, H.B., Kastelein, J.J., Hu, B., Uno, K., Kataoka, Y.*, et al.* (2016). Effect of the BET Protein Inhibitor, RVX-208, on Progression of Coronary Atherosclerosis: Results of the Phase 2b, Randomized, Double-Blind, Multicenter, ASSURE Trial. American journal of cardiovascular drugs : drugs, devices, and other interventions *16*, 55-65.10.1007/s40256-015-0146-z

Nicholls, S.J., Schwartz, G.G., Buhr, K.A., Ginsberg, H.N., Johansson, J.O., Kalantar-Zadeh, K., Kulikowski, E., Toth, P.P., Wong, N., Sweeney, M.*, et al.* (2021). Apabetalone and hospitalization for heart failure in patients following an acute coronary syndrome: a prespecified analysis of the BETonMACE study. Cardiovascular diabetology *20*, 13.10.1186/s12933-020-01199-x

Nicodeme, E., Jeffrey, K.L., Schaefer, U., Beinke, S., Dewell, S., Chung, C.W., Chandwani, R., Marazzi, I., Wilson, P., Coste, H.*, et al.* (2010). Suppression of inflammation by a synthetic histone mimic. Nature *468*, 1119-1123.10.1038/nature09589

Nishiga, M., Wang, D.W., Han, Y., Lewis, D.B., and Wu, J.C. (2020). COVID-19 and cardiovascular disease: from basic mechanisms to clinical perspectives. Nature Reviews Cardiology.10.1038/s41569-020-0413-9

Oladunni, F.S., Park, J.G., Pino, P.A., Gonzalez, O., Akhter, A., Allué-Guardia, A., Olmo-Fontánez, A., Gautam, S., Garcia-Vilanova, A., Ye, C.*, et al.* (2020). Lethality of SARS-CoV-2 infection in K18 human angiotensin-converting enzyme 2 transgenic mice. Nature communications *11*, 6122.10.1038/s41467-020-19891-7

Orlova, V.V., van den Hil, F.E., Petrus-Reurer, S., Drabsch, Y., Ten Dijke, P., and Mummery, C.L. (2014). Generation, expansion and functional analysis of endothelial cells and pericytes derived from human pluripotent stem cells. Nat Protoc *9*, 1514-1531.10.1038/nprot.2014.102

Padmanabhan, A., Alexanian, M., Linares-Saldana, R., González-Terán, B., Andreoletti, G., Huang, Y., Connolly, A.J., Kim, W., Hsu, A., Duan, Q.*, et al.* (2020). BRD4 (Bromodomain-Containing Protein 4) Interacts with GATA4 (GATA Binding Protein 4) to Govern Mitochondrial Homeostasis in Adult Cardiomyocytes. Circulation *142*, 2338-2355.10.1161/circulationaha.120.047753

Pellegrini, D., Kawakami, R., Guagliumi, G., Sakamoto, A., Kawai, K., Gianatti, A., Nasr, A., Kutys, R., Guo, L., Cornelissen, A.*, et al.* (2021). Microthrombi As A Major Cause of Cardiac Injury in COVID-19: A Pathologic Study. Circulation.10.1161/circulationaha.120.051828

Puntmann, V.O., Carerj, M.L., Wieters, I., Fahim, M., Arendt, C., Hoffmann, J., Shchendrygina, A., Escher, F., Vasa-Nicotera, M., Zeiher, A.M.*, et al.* (2020). Outcomes of Cardiovascular Magnetic Resonance Imaging in Patients Recently Recovered From Coronavirus Disease 2019 (COVID-19). JAMA Cardiology.10.1001/jamacardio.2020.3557

Qiao, Y., Wang, X.-M., Mannan, R., Pitchiaya, S., Zhang, Y., Wotring, J.W., Xiao, L., Robinson, D.R., Wu, Y.-M., Tien, J.C.-Y.*, et al.* (2021). Targeting transcriptional regulation of SARS-CoV-2 entry factors ACE2 and TMPRSS2. Proceedings of the National Academy of Sciences *118*, e2021450118.10.1073/pnas.2021450118

1 Quaife-Ryan, G.A., Sim, C.B., Ziemann, M., Kaspi, A., Rafehi, H., Ramialison, M., El-Osta, A., Hudson, J.E.,
2 and Porrello, E.R. (2017). Multicellular Transcriptional Analysis of Mammalian Heart Regeneration.
3 Circulation *136*, 1123-1139.10.1161/circulationaha.117.028252
4 Ray, K.K., Nicholls, S.J., Buhr, K.A., Ginsberg, H.N., Johansson, J.O., Kalantar-Zadeh, K., Kulikowski, E.,
5 Toth, P.P., Wong, N., Sweeney, M., *et al.* (2020). Effect of Apabetalone Added to Standard Therapy on
6 Major Adverse Cardiovascular Events in Patients With Recent Acute Coronary Syndrome and Type 2
7 Diabetes: A Randomized Clinical Trial. Jama *323*, 1565-1573.10.1001/jama.2020.3308
8 Ren, X., Wen, W., Fan, X., Hou, W., Su, B., Cai, P., Li, J., Liu, Y., Tang, F., Zhang, F., *et al.* (2021). COVID-19
9 immune features revealed by a large-scale single cell transcriptome atlas.
10 Cell.10.1016/j.cell.2021.01.053
11 Richardson, P., Griffin, I., Tucker, C., Smith, D., Oechsle, O., Phelan, A., Rawling, M., Savory, E., and
12 Stebbing, J. (2020). Baricitinib as potential treatment for 2019-nCoV acute respiratory disease. Lancet
13 *395*, e30-e31.10.1016/S0140-6736(20)30304-4
14 Robinson, M.D., McCarthy, D.J., and Smyth, G.K. (2010). edgeR: a Bioconductor package for differential
15 expression analysis of digital gene expression data. Bioinformatics (Oxford, England) *26*, 139-
16 140.10.1093/bioinformatics/btp616
17 Runte, K.E., Bell, S.P., Selby, D.E., Häußler, T.N., Ashikaga, T., LeWinter, M.M., Palmer, B.M., and Meyer,
18 M. (2017). Relaxation and the Role of Calcium in Isolated Contracting Myocardium From Patients With
19 Hypertensive Heart Disease and Heart Failure With Preserved Ejection Fraction. Circ Heart Fail
20 *10*.10.1161/circheartfailure.117.004311
21 Rzymski, T., Mikula, M., Żyłkiewicz, E., Dreas, A., Wiklik, K., Gołas, A., Wójcik, K., Masiejczyk, M., Wróbel,
22 A., Dolata, I., *et al.* (2017). SEL120-34A is a novel CDK8 inhibitor active in AML cells with high levels of
23 serine phosphorylation of STAT1 and STAT5 transactivation domains. Oncotarget *8*, 33779-
24 33795.10.18632/oncotarget.16810
25 Sadzak, I., Schiff, M., Gattermeier, I., Glinitzer, R., Sauer, I., Saalmüller, A., Yang, E., Schaljo, B., and
26 Kovarik, P. (2008). Recruitment of Stat1 to chromatin is required for interferon-induced serine
27 phosphorylation of Stat1 transactivation domain. Proceedings of the National Academy of Sciences of
28 the United States of America *105*, 8944-8949.10.1073/pnas.0801794105
29 Sanders-van Wijk, S., Tromp, J., Beussink-Nelson, L., Hage, C., Svedlund, S., Saraste, A., Swat, S.A.,
30 Sanchez, C., Njoroge, J., Tan, R.S., *et al.* (2020). Proteomic Evaluation of the Comorbidity-Inflammation
31 Paradigm in Heart Failure With Preserved Ejection Fraction: Results From the PROMIS-HFpEF Study.
32 Circulation *142*, 2029-2044.10.1161/circulationaha.120.045810
33 Schumacher, S.M., Gao, E., Zhu, W., Chen, X., Chuprun, J.K., Feldman, A.M., Tesmer, J.J.G., and Koch,
34 W.J. (2015). Paroxetine-mediated GRK2 inhibition reverses cardiac dysfunction and remodeling after
35 myocardial infarction. Science translational medicine *7*, 277ra231-
36 277ra231.10.1126/scitranslmed.aaa0154
37 Sharma, A., Garcia, G., Jr., Wang, Y., Plummer, J.T., Morizono, K., Arumugaswami, V., and Svendsen, C.N.
38 (2020). Human iPSC-Derived Cardiomyocytes Are Susceptible to SARS-CoV-2 Infection. Cell Rep Med *1*,
39 100052-100052.10.1016/j.xcrm.2020.100052
40 Shi, S., Qin, M., Shen, B., Cai, Y., Liu, T., Yang, F., Gong, W., Liu, X., Liang, J., Zhao, Q., *et al.* (2020).
41 Association of Cardiac Injury With Mortality in Hospitalized Patients With COVID-19 in Wuhan, China.
42 JAMA Cardiology *5*, 802-810.10.1001/jamacardio.2020.0950
43 Stratton, M.S., Bagchi, R.A., Felisbino, M.B., Hirsch, R.A., Smith, H.E., Riching, A.S., Enyart, B.Y., Koch,
44 K.A., Cavasin, M.A., Alexanian, M., *et al.* (2019). Dynamic Chromatin Targeting of BRD4 Stimulates
45 Cardiac Fibroblast Activation. Circulation research *125*, 662-677.doi:10.1161/CIRCRESAHA.119.315125
46 Stubbs, M.C., Burn, T.C., Sparks, R., Maduskuie, T., Diamond, S., Rupar, M., Wen, X., Volgina, A.,
47 Zolotarjova, N., Waeltz, P., *et al.* (2019). The Novel Bromodomain and Extraterminal Domain Inhibitor

47

1 INCB054329 Induces Vulnerabilities in Myeloma Cells That Inform Rational Combination Strategies.
2 Clinical Cancer Research *25*, 300-311.10.1158/1078-0432.ccr-18-0098
3 Szekely, Y., Lichter, Y., Taieb, P., Banai, A., Hochstadt, A., Merdler, I., Oz, A.G., Rothschild, E., Baruch, G.,
4 Peri, Y.*, et al.* (2020). The Spectrum of Cardiac Manifestations in Coronavirus Disease 2019 (COVID-19) -
5 a Systematic Echocardiographic Study. Circulation *0*.doi:10.1161/CIRCULATIONAHA.120.047971
6 Tucker, N.R., Chaffin, M., Fleming, S.J., Hall, A.W., Parsons, V.A., Jr, K.C.B., Akkad, A.-D., Herndon, C.N.,
7 Arduini, A., Papangeli, I.*, et al.* (2020). Transcriptional and Cellular Diversity of the Human Heart.
8 Circulation *0*.doi:10.1161/CIRCULATIONAHA.119.045401
9 Tyanova, S., and Cox, J. (2018). Perseus: A Bioinformatics Platform for Integrative Analysis of Proteomics
10 Data in Cancer Research. Methods in molecular biology (Clifton, NJ) *1711*, 133-148.10.1007/978-1-4939-
11 7493-1_7
12 Vasudevan, N.T., Mohan, M.L., Gupta, M.K., Martelli, E.E., Hussain, A.K., Qin, Y., Chandrasekharan, U.M.,
13 Young, D., Feldman, A.M., Sen, S.*, et al.* (2013). Gβγ-independent recruitment of G-protein coupled
14 receptor kinase 2 drives tumor necrosis factor α-induced cardiac β-adrenergic receptor dysfunction.
15 Circulation *128*, 377-387.doi:10.1161/CIRCULATIONAHA.113.003183
16 Voges, H.K., Mills, R.J., Elliott, D.A., Parton, R.G., Porrello, E.R., and Hudson, J.E. (2017). Development of
17 a human cardiac organoid injury model reveals innate regenerative potential. Development (Cambridge,
18 England) *144*, 1118-1127.10.1242/dev.143966
19 Williams, L.M., McCann, F.E., Cabrita, M.A., Layton, T., Cribbs, A., Knezevic, B., Fang, H., Knight, J., Zhang,
20 M., Fischer, R.*, et al.* (2020). Identifying collagen VI as a target of fibrotic diseases regulated by
21 CREBBP/EP300. Proceedings of the National Academy of Sciences of the United States of America *117*,
22 20753-20763.10.1073/pnas.2004281117
23 Wolf, F.A., Angerer, P., and Theis, F.J. (2018). SCANPY: large-scale single-cell gene expression data
24 analysis. Genome biology *19*, 15.10.1186/s13059-017-1382-0
25 Wu, Z., and McGoogan, J.M. (2020). Characteristics of and Important Lessons From the Coronavirus
26 Disease 2019 (COVID-19) Outbreak in China: Summary of a Report of 72 314 Cases From the Chinese
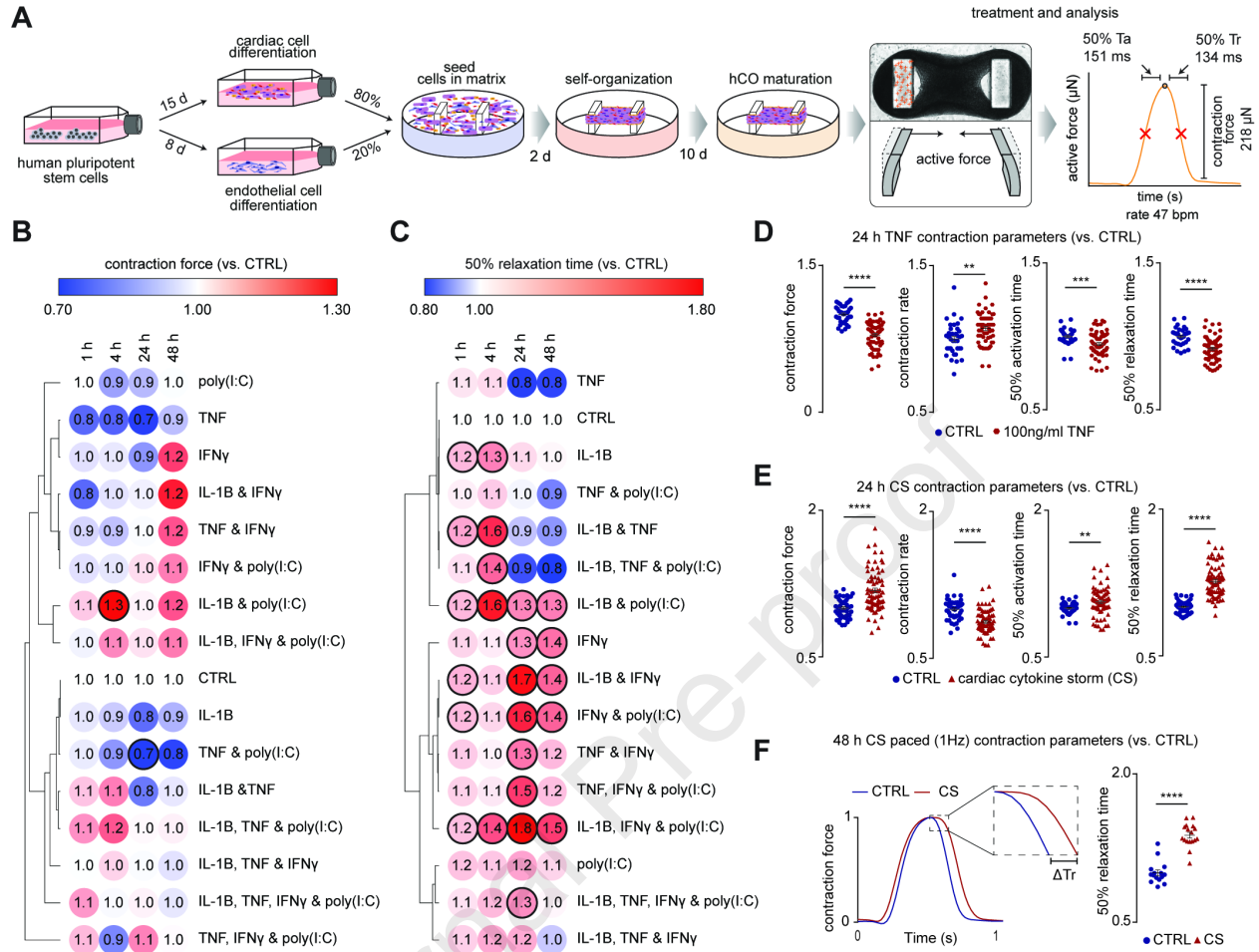27 Center for Disease Control and Prevention. JAMA *323*, 1239-1242.10.1001/jama.2020.2648

28

HIGHLIGHTS and eTOC BLURB

Highlights

- Pro-inflammatory factors drive systolic and diastolic cardiac dysfunction
- BRD4 activation drives diastolic dysfunction and is blocked by clinically relevant drugs
- BET inhibition decreases ACE2 expression and decreases SARS-CoV2 infection

eTOC Blurb

A combination of phosphoproteomics, drug screening and single-cell sequencing approaches identifies how cytokines elevated in COVID-19 patients drives cardiac dysfunction, with BET inhibitors serving as potential lead candidates decrease ACE2 cardiac expression and infection.

A

global phosphoproteomics screen for hCO cytokine storm drug candidates

CTRL

cardiac cytokine storm
n = 3

high-sensitivity phosphoproteomics
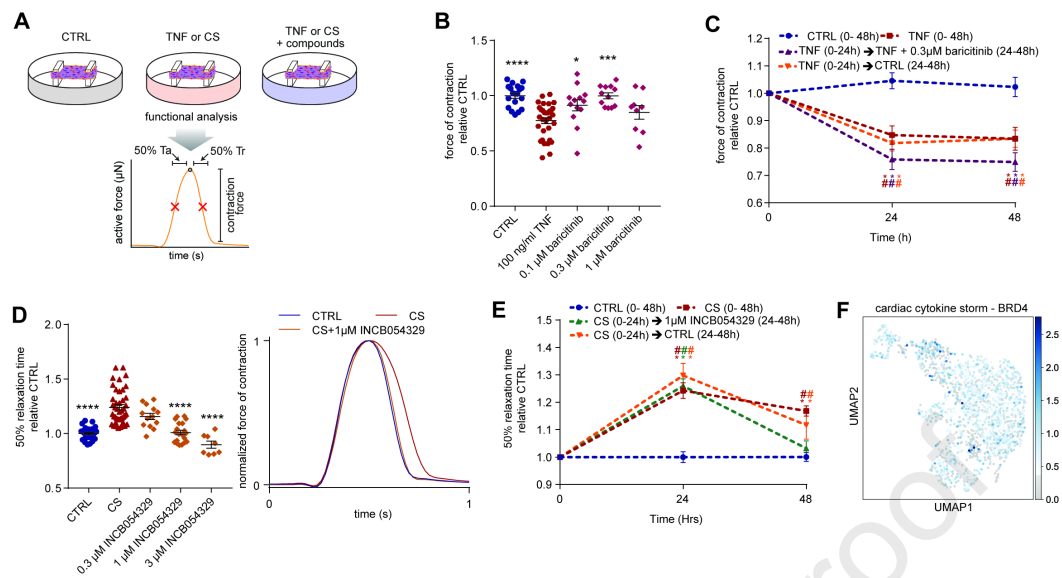
EasyPhos

LC — 60 min gradient 40 cm column — ESI — single-run QE HF-X — MS

MaxQuant

2,981 phosphoproteins
9,513 phosphopeptides
7,927 phosphosites (class 1)

replicate outlier detection

density

fold-change
-5   0   5

B

CTRL

CS

TF/TA

Phosphopeptide response (log2 fold change)
-4   0   4

C

STAT1

1   136   317   573   670   750
N   COIL   SH2   C
727 ⑤
↑
CDK8

BRD4

binds
G9a
P-TEFb

1   75   147   368   440   600   682   1362
N   BD1   BD2   NET   CTD   C
469 ⑤   1083 ⑤
↑   ↑
?   ?

BETi and BD2 targeting prevent diastolic dysfunction caused by cardiac cytokine storm

A

50% relaxation time rel CTRL

CTRL, CS, 1 μM INCB054329, 3 μM JQ-1, 10 μM JQ-1, 1 μM ABBV-744, 1 μM molibresib, 3 μM molibresib, 1 μM alobresib, 3 μM apabetalone, 10 μM apabetalone, 30 μM apabetalone

B

50% relaxation time rel CTRL

CTRL, CS, 1 μM apabetalone, 5 μM apabetalone, 25 μM apabetalone, 1 μM RVX-2157, 5 μM RVX-2157, 25 μM RVX-2157

C

ASSURE phase IIb
(NCT01067820)

LGALS3BP change (%)

placebo, apabetalone
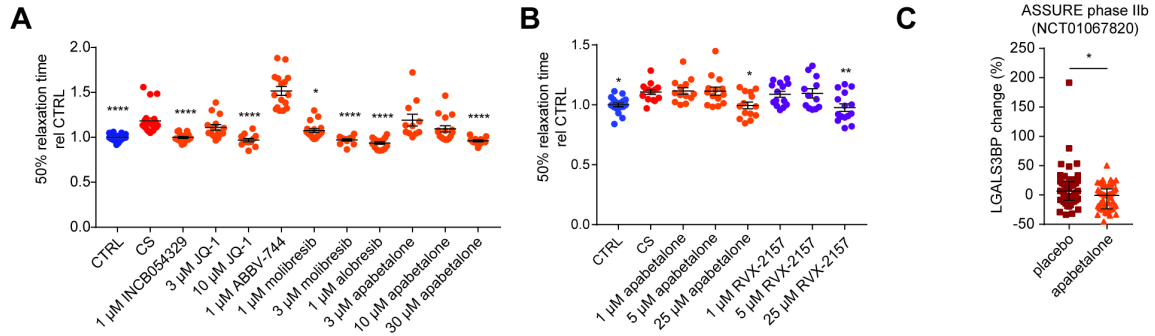
BETi and BD2 targeting reduce ACE2 and SARS-CoV-2 infection

D

DMSO, 25 μM apabetalone, 25 μM RVX-2157

ACE2 (110 kDa)

GAPDH (37 kDa)

E

$SARS\text{-}COV\text{-}2\ E/18S$ rel DMSO

CTRL, DMSO, 25 μM apabetalone, 25 μM RVX-2157

F

$SARS\text{-}COV\text{-}2\ E/18S$ rel DMSO

DMSO, [apabetalone] (μM): 0.1, 0.3, 1, 3, 10, 30

G

virus titre log10(TCID50/mL)

DMSO, 3 μM JQ-1, 30 μM apabetalone